OCCAM

OXFORD CENTRE FOR COLLABORATIVE APPLIED MATHEMATICS

A Review of Mathematical Models for the Formation of Vascular Networks

by

M. Scianna
C. Bell
L. Preziosi

OCCAM Preprint Number 12/78

A Review of Mathematical Models for the Formation of Vascular Networks

M. Scianna*, C. Bell†, and L. Preziosi*

Abstract

Mainly two mechanisms are involved in the formation of blood vasculature: vasculogenesis and angiogenesis. The former consists of the formation of a capillary-like network from either a dispersed or a monolayered population of endothelial cells, reproducible also *in vitro* by specific experimental assays. The latter consists of the sprouting of new vessels from an existing capillary or post-capillary venule. Similar phenomena are also involved in the formation of the lymphatic system through a process generally called lymphangiogenesis.

A number of mathematical approaches have analysed these phenomena. This paper reviews the different modelling procedures, with a special emphasis on their ability to reproduce the biological system and to predict measured quantities which describe the overall processes. A comparison between the different methods is also made, highlighting their specific features.

Keywords: continuous model – mechanical model - hybrid models – cellular Potts model – vasculogenesis - angiogenesis -lymphangiogenesis

Introduction

Blood vessel formation and development is a multiscale process, driven by the activation of endothelial cells (ECs, the main bricks of the capillary walls) induced by the action of suitable biochemical stimuli which are released both by environmental cells and by ECs themselves. Vascular progression involves two different mechanisms: vasculogenesis and angiogenesis (for a review, see [39, 43, 44]). The former process mainly consists in the formation of a primitive vascular network, that emerges from a directed and autonomous migration, aggregation and organization of the endothelial cells. The latter consists instead of the formation of new vessels from an existing capillary or post-capillary venule. Angiogenic remodelling co-ordinates with the establishment of blood flow and can occur through sprouting, i.e., by the formation of new branches from the sides of existing capillaries, pruning, resizing of the capillary volume of of the thickness of the capillary wall, or intussusception, i.e., by internal division of the vessel lumen.

*Dip. Scienze Matematiche, Politecnico di Torino, Corso degli Abruzzi 24, 10129, Torino, Italy.

†Mathematical Institute, University of Oxford, 24-29 St Giles', Oxford, OX1 3LB, UK.

Entering into more detail, in the embryo, the process of vasculogenesis starts with the assembly of mesoderm-derived precursors of ECs [175] in polygons having well determined topological characteristics, dictated by the principal and paradigmatic function of vasculature: the oxygen transport to the tissues. After remodelling, these geometrical properties are more or less maintained in the adult body, where the capillary network embedded in the tissues and stemmed by the vascular tree has the same shape as the minimal unit participating in the formation of the embryo vascular net [49, 86, 107].

Though angiogenesis already intervenes in the embryo to remodel the initial capillary network into a mature and functional vascular bed comprised of arteries, capillaries, and veins, its main role is played during the adult life, when it is involved in many physiological processes, for instance, the vascularization of the ovary and the uterus during the female cycle, of the mammary gland during lactation and of granulation tissues after wound healing. However, when the equilibrium of its underlying control mechanisms is disrupted, angiogenesis becomes pathological, as in the cases of chronic inflammatory diseases like rheumatoid arthritis and psoriasis, vasculopathies like diabetic microangiopathy, degenerative disorders like atherosclerosis and cirrhosis, tissue injury occurring in ischemia. Indeed, the angiogenic progression is a pivotal transition also in cancer development. In fact by providing the nutrition and oxygen, it allows malignant cells to grow and remain viable, and, eventually, to cause metastases and invasion of the circulatory system [44]. Moreover, it is also active in determining the translation of dormant metastases to an aggressive status [43]. The switch to the angiogenic phenotype leads therefore to a fast progression and to a potentially fatal stage of the disease and represents an important target for therapeutic interventions in most types of malignancies [195].

The understanding of angiogenesis and vasculogenesis is indeed of particular importance in cancer therapy on the one side for the research of anti-angiogenic therapies, and on the other for the optimisation of drug delivery to tumour sites. In fact, counter-intuitively Jain and co-workers [79, 97, 98] hypothesized that, in order to achieve a better delivery of drugs, it is important to normalise the vascular network through the restoration of a proper balance of pro-angiogenic and anti-angiogenic factors. In this way, a usually abnormal tumour vasculature can be normalized improving perfusion, oxygenation and overall efficacy, and also allowing a reduction of tumour interstitial pressure, a further factor hampering drug delivery to the tumour site.

Recently, there is a growing interest in governing the formation of capillary networks in order to construct in vitro tissues already with embedded capillaries. In fact, the growth of 3D tissues had scarce results due to the fact that it is limited by the diffusion of nutrients inside the scaffold. Even in the case of a successful growth in vitro obtained by carefully forcing a flow through the scaffold, it is very difficult to successfully implant the artificial tissue in the body because of the absence of a capillary network, so that the tissue usually becomes necrotic because of the lack of nutrients. Providing the scaffold with a network or stimulating its development together with the host tissue would instead allow bigger 3D tissues to be built and more successful implants to be achieved (see, for instance, [45, 56, 84, 95, 99, 110, 135, 196, 211, 214]). In particular, Stroock and co-workers [232] developed a micro-fluidic device embedded in a tissue-like collagen matrix where ECs can grow on the inner walls of the micro-channels, forming the first capillaries. The 3D matrix surrounding the vessels and the

flow allowed for the cells themselves to adapt the structure to a physiological one and even to form new sprouts, which is very important in view of forming connections with the tissue that is going to host the part grown in vitro.

The experimental studies performed on both the tubulogenic system and the vasculogenic system and on their driving mechanisms has revealed the role of different factors operating in vascular progression, both in physiological conditions and in pathological situations. However, innumerable other processes, acting at different spatio-temporal scales, are far from being completely elucidated. Their complexity presents indeed a number of components which is obviously impossible to study using only laboratory-based biological methods, but which can be more efficiently analysed by *in silico* models, able to replicate selected features of the experimental system.

The aim of this review is to present the different approaches, i.e., continuous, mechanics-based, hybrid, and cell-based models, used to model the formation of vascular networks, with a special emphasis on their ability to reproduce the experimental system and to predict measured quantities. In doing that more attention will be paid to the results obtained in the last ten years, referring to [8, 11, 117, 123] for further details on previous contributions. Some sample models will be explained in detail in order to make more evident the modelling differences. Finally, a comparison between the different methods will be done, putting in evidence their specific features with their advantages and disadvantages.

1 *In vitro* vasculogenesis

Given the fundamental importance of vessel formation and reorganization, a large amount of in vitro assays have been advanced to provide a deeper understanding of selected underpinning molecular-scale and cellular-scale events. One of the most known is the tubulogenic experiment, the laboratory counterpart of *in vivo* vasculogenesis (see Figure 1). Tubulogenic assays can be obtained using different experimental set-ups, substrata (e.g., Matrigel, fibronectin, collagen, fibrin, semisolid methilcellulose), and endothelial cell-lines (e.g., human umbilical vein endothelial cells (HUVEC), human dermal microvascular endothelial cells (HDMEC), human capillary endothelial cells (HCEC), human marrow microvascular endothelial cells, bovine aorthic endothelial cells (BAEC), bovine capillary endothelial cells (BCEC), bovine retin endothelial cells (BREC), rat capillary endothelial cells (RCEC), embryonic stem cells (ESC), calf pulmonary aortic endothelial cells (CPAEC), adrenal capillary endothelial cells (ACEC)), as reviewed in [212].

Recent experimental investigations have demonstrated that, from the macroscopic morphological analysis, tumour blood vessels are irregular and dilated and that distinct venules, arterioles, and capillaries are undistinguishable [54, 73]. Moreover, they differ from their "normal" counterpart by their altered blood flow and permeability, and by abnormalities in pericytes and in the basement membrane. Therefore, in recent years, an increasing number of vasculogenic assays have been performed with tumour-derived endothelial cell lines (TECs), isolated and cultured from human carcinomas on the basis of membrane markers. Indeed, they exhibit altered genotype, phenotype, and function, are often aneuploid and display chromosomal instability and express peculiar genes [38,

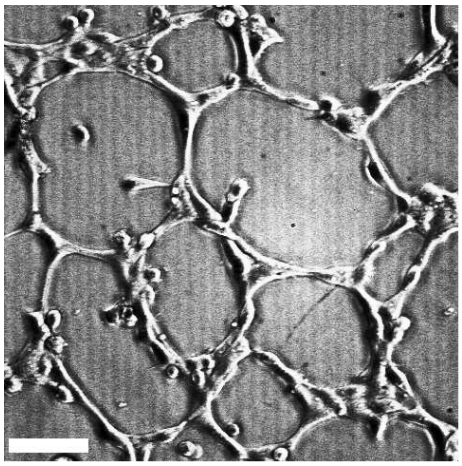

Figure 1: In vitro vasculogenesis.

158, 186]. In addition, TECs avoid senescence *in vitro* and show enhanced proliferation, motility and over-expression of membrane receptors [22, 36, 37, 38, 82]. Therefore, TECs represent a more adequate model for studying the mechanisms of malignant vascularization and for testing the efficacy of anti-angiogenic pharmacological therapies and drugs.

In spite of such a large variety of laboratory protocols mentioned above, it is possible to point out a unified illustration of the common features of the experimental process. The selected EC population is initially dispersed in a physiological solution and then poured on the top of a specific substrate, which typically favours cell motility and has biochemical characteristics similar to living tissues. The cells sediment by gravity onto the surface and then move on it, giving rise to the mechanisms of aggregation and pattern formation. In more detail, the overall process, which commonly lasts 9-15 hours, consists of the following steps:

1. Cells initially undergo an isotropic motion around their initial position, maintaining a round shape. Then, it seems that they choose a direction, which is correlated with the location of areas characterized by higher cellular densities, and display an independent migration, with a small random component, until they collide with their closest neighbours (3-6 hours). This motile phenotype is called in biology cell persistence and is related to the inertia of a cell in rearranging and repolarizing its cytoskeleton, maintaining its own direction of migration [71, 179]. It is interesting to remark that in this phase cells move significantly fast and their movement seems to be of *amoeboid* type, which can be compared with the exhibition of a gymnast with a quick sequence of jumps (refer, for instance, to [221, 228]).

2. After collision, ECs attach to their neighbours eventually forming a continuous multicellular network, which can be represented as a collection of nodes connected by capillary chords. Concomitantly, the number of adhesion sites with the substrate increases and the ECs achieve an even

more elongated shape. In this stage, the motion, which is of mesenchymal type, is much slower and resembles that of a mountain-climber, who uses as many footholds as possible, grabbing new contact points and detaching from old ones one at a time.

3. The network slowly moves as a whole, undergoing a slow thinning process, which however leaves the structure mainly unaltered. During this stabilization phase the mechanical interactions among cells, and between cells and the substratum, become important.

4. Finally, individual cells fold up to origin the lumen of the capillary, so that the resulting vascular network forms along the lines of the previous, as described in [83, 108].

1.1 Activity of chemical morphogens and relative intracellular pathways

As explained in the previous section, the motion of cells in the first phase of the patterning seems to be well established toward the region characterized by higher cell densities. A natural question is indeed how the cells feel the presence of other cells, i.e., what is the mechanism underlying intracellular cross-talk. In this regard, recent works clearly confirm that endothelial cells exchange signals during vasculogenesis by the release and absorption of specific chemical morphogens, such as vascular endothelial growth factor isoforms (VEGF-A), acidic and basic fibroblast growth factors (FGFs), epidermal growth factor (EGF), transforming growth factor-α and -β (TGF-α and -β), as for instance reviewed in [43, 60, 89]. These angiogenic factors, which are known to induce ECs growth, survival, and motility [61, 151], can in fact bind to specific tyrosine kinase receptors on the cell surface and induce chemotactic motion along their concentration gradient, i.e., towards zones of higher cellular densities.

In order to quantify both the persistent and the chemotactic component in cell motion, in [10, 159, 182, 187] a statistical analysis of the cell trajectories is performed, measuring the displacement between successive turns and the accumulative distance. In particular, Parsa et al. [159] and Serini et al. [187] measure both the angle between two subsequent displacements relative to the same trajectory, which gives a measure of the persistence, and the angle between the cell instantaneous velocity and the VEGF-A concentration gradients at the same point, which gives a measure of the chemotactic behaviour. Indeed, they observe and confirm a persistence of cell locomotion in time and an alignment of the migration with the direction of the gradients of the concentration field.

The autocrine/paracrine growth factors play also a role in determining the dimensions of the overall network. In particular, different types of morphogens can lead to different mesh sizes, as observed in [177], where mice lacking heparin-binding isoforms of VEGF-A form vascular networks with a larger structure. As discussed in the sequel, and proved by different theoretical models [74, 187], this is related to the fact that the typical size of the network is determined by the product of the diffusion constant and the half-life of the chemical factor, which are affected by its molecular weight and therefore specific for each chemical species. In [85] it is clearly shown how eliminating endogenous VEGF-A, the ECs plated on Matrigel do not form networks even when VEGF-A is added exhogenously and homogeneously on the top of the layer.

The diffusive chemical morphogens not only exert a chemotactic action on the ECs but, concomitantly, also activate a series of calcium-dependent cascades, regulating the phenotypical behaviour of cells, e.g. motility, that is in turn influenced by cell-to-cell contact. Their role then becomes essential for the stabilization of the capillary network. Molecules of selected growth factors initiate a series of intracellular cascades, which results in the indirect production of second messengers (such as arachidonic acid (AA) and nitric oxide (NO)), which, binding to sites on cell plasmamembrane, open cation channels and allow the influx of extracellular calcium into the cytosol, as characterized in [63, 64, 65, 136, 140]. The process, also called non-capacitive (or non-store-operated) calcium entry (NCCE or NSOCE), causes localized and peripheral restricted accumulations of the ion [206], which regulate important biophysical properties of vascular cells, such as their elasticity, migratory capacity and adhesive strength [28, 139, 141, 143].

1.2 Topological properties of the network and relative dependence on cell density and substrate thickness

Several experimental approaches clearly show that, over a defined range of densities of seeded cells (say from 100 to 200 cells/mm^2), the resulting network is characterized by typical inter-capillary distances (i.e., mean diameter of cellular lacunae), extending from 50 to 300 μm. These dimensions are instrumental for optimal metabolic exchange (determined by the diffusivity of the oxygen): a coarser net would in fact cause necrosis of the tissues in the central region, a finer net would instead be useless (see [49, 86]). Indeed, as observed *in vivo* in [69], outside these values of cell density, the vascular mesh does not develop properly. To enlighten this phenomenon, Serini and co-workers [187] performed specific experiments varying the number of seeded cells, and used methods of statistical mechanics to quantitatively characterize the resulting patterns [74, 50]. As a result, one can observe a transition between a phase in which dynamics generates several disconnected structures (i.e., below a critical value $\sim$ 100 cells/mm^2) to a phase in which a single connected structure appears. This process is an example of percolative transition and is studied in detail in [50].

A detailed analysis of the topological parameters characterizing the network such as average branch length, number of branches, number of nodes, or capillary-like structure area was performed in [159]. The same article also devotes a particular attention to the evolution of the shapes of single endothelial cells. They characterize cell behaviour in five phases dominated by cell aggregation, spreading, elongation, plexus stabilization, plexus reorganization.

When too many cells are seeded, another transition, called Swiss-cheese transition, is observed with the formation of regions without cells, called lacunae, in a confluent layer of undifferentiated ECs, that therefore do not form a proper network.

The topological properties of the capillary network are strictly regulated also by the content of matrix proteins in the substrate, which regulate cell attachment over the gel surface. In particular, experimental observations have pointed out that lacunae form in the zones deprived of ECM molecules [209]. Indeed, in [212], the authors noticed that the formation of cellular holes was accompanied by a degradation of fibrin gels: in more detail, they measured the fibrin degradation products present in the culture medium and found an in-

crease after 10 hours of seeding HUVECs. The same group has also performed some experiments changing the fibrin concentration in a substratum of 1 mm thickness with a confluent population of HUVECs (i.e., with a density ≈ 1500 cells/mm^2). Increasing the fibrin concentration from 0.5 mg/mL to 8 mg/mL, the number of formed lacunae strongly decreased, without increasing in size. In particular, a structured capillary mesh, with a typical chord length of $550 \pm 50\mu$m, only formed for lower fibrin concentrations. At higher values, the ensemble of cells remained in fact a continuous carpet without holes. These results suggested that fibrinolysis leads to cell apoptosis, and detachment from the surface, during the process, eventually resulting in the formation of functional lacunae. The same researchers have repeated the experiments using BRECs: in this case, a higher fibrin concentration (≈ 8 mg/mL) was necessary to form an organized capillary network, with a mean chord length of 400μm. This is consistent with the fact that BRECs present a high fibrinolytic activity so that, at lower concentration, the matrix gel is degraded too quickly and the cells could not adhere at all. For this reason, some experiments were performed adding protease inhibitors (aprotin up to a concentration of 1 μg/mL), which decreased the degradation and allowed the formation of capillary-like structures. However, the fibrin degradation had been completely inhibited, the capillary network no longer formed.

The interaction between cells and ECM during tubulogenesis has been the subject of many experiments: in [215, 216, 217], the authors seeded different types of cells (i.e., BAEC, cells of the murine Leydig cell line TM3, human fibroblasts, human smooth muscle cells, and murine PYS-2 cells) on gelled basement membrane matrices (BBMs), characterized by a constant thickness of 1 mm and a variable rigidity, regulated by selected amounts of gelled native type I collagen. They found that, with 0.6mg/mL collagen, BAEC and TM3 cells formed capillary networks in 24 hours, whereas, at 2mg/mL collagen, cells were flattened, spread, and unorganised. In addition, they used a set-up in which the substratum was distributed with a triangular shape increasing from 10 μm to 500 μm over a length of 17 mm or from 10 μm to 400 μm over a length of 4 mm: the experiment showed the formation of longer chords in the case of high thickness and of shorter chords in the opposite situation. Probably, on an even thinner substrate, a capillary structure would have not formed at all.

2 Continuous models of vasculogenesis

The first mathematical models aimed at describing vasculogenesis were developed in the eighties by Murray and co-workers [144, 145, 146, 155], then followed by a series of papers [121, 122, 147, 148, 149, 150, 209] reviewed in more detail in [11, 123]. This type of models was based on the assumption that the mechanism driving the formation of the vascular network and its morphological characteristics was the pulling action of cells on the extracellular matrix (ECM).

Denoting by ρ_c the density of endothelial cells, by ρ_m the density of ECM, and by $\mathbf{u}_m$ the displacement of the extracellular matrix with respect to its

stress-free configuration, the structure of the model is the following

$$\frac{\partial \rho_c}{\partial t} + \nabla \cdot \mathbf{J}_c = 0\,, \tag{2.1}$$

$$\frac{\partial \rho_m}{\partial t} + \nabla \cdot (\rho_m \mathbf{v}_m) = 0, \tag{2.2}$$

$$\nabla \cdot (\mathbf{T}_c + \mathbf{T}_m) = \mathbf{F}\,, \tag{2.3}$$

where $\mathbf{v}_m = d\mathbf{u}_m/dt$ is the ECM velocity, $\mathbf{J}_c$ is the cellular flux, $\mathbf{T}_c$ is called "cell traction stress" and $\mathbf{T}_m$ is the stress in the deformed ECM. Finally, $\mathbf{F}$ is the force due to the interaction between the ECM and the Petri-dish. So, Eqs. (2.1) and (2.2) write as conservation equations for the cell and ECM density, while the last equation is a force balance equation for the whole system, the mixture of cells and Matrigel. The term $\mathbf{T}_c$ accounts for the forces internal to the system due to the cell traction; $\mathbf{T}_m$ accounts for the viscoelastic response of the ECM.

Actually, in [121] a growth term $\Gamma_c = \gamma_c \rho_c$ was introduced in the r.h.s. of Eq. (2.1) to describe cell proliferation, but was then neglected in the stability analysis and in the simulation. Similarly, in [209] a decay term $\Delta = -\delta_m \rho_c (1 - \rho_c)\rho_m$ was introduced in the r.h.s. of Eq. (2.2) to account for ECM cleavage by the ECs, that was assumed to play a role in the formation of lacunae.

On the basis of the experimental evidence mentioned in Section 1.1 showing the importance of chemical cues especially during the first phase of vascular development, [12, 74, 187] developed a mathematical model based on the following assumptions:

- ECs neither duplicate nor die during the process;
- ECs communicate via the release and absorption of molecules of a soluble growth factor, which acts as a chemoattractant and can reasonably identified with VEGF-A;
- ECs show persistence in their motion;
- Cells are slowed down by friction due to the interaction with the fixed substratum;
- Closely packed cells mechanically respond to avoid overcrowding.

The resulting mathematical model for the density of cells, ρ_c, their velocity, $\mathbf{v}_c$, and the concentration of chemoattractant, c, then writes as:

$$\frac{\partial \rho_c}{\partial t} + \nabla \cdot (\rho_c \mathbf{v}_c) = 0\,, \tag{2.4}$$

$$\frac{\partial c}{\partial t} = D\nabla^2 c + \alpha \rho_c - \frac{c}{\tau}\,, \tag{2.5}$$

$$\rho_c \left(\frac{\partial \mathbf{v}_c}{\partial t} + \mathbf{v}_c \cdot \nabla \mathbf{v}_c \right) = \nabla \cdot \mathbf{T}_c + \mathbf{F}_{chem} + \mathbf{F}_{cm}\,. \tag{2.6}$$

As above, Eq. (2.4) is a mass conservation equation corresponding to the above-explained assumption that cells do not undergo mitosis or apoptosis during the experimental phenomenon.

Equation (2.5) is a diffusion equation for the chemical factor which is produced at a rate α and degrades with a half life τ. The diffusion coefficient can be estimated from available data of molecular radii [137, 218] using the Einstein-Stokes relation $D = k_{\mathrm{B}}T/(6\pi\eta r_{\mathrm{H}})$ where k_{B} is Boltzmann's constant, T the temperature, η the solvent viscosity, r_{H} the hydrodynamic radius of the molecule [167]. In the case of VEGF-A, this gives $D \sim 10^{-7}\,\mathrm{cm}^2\,\mathrm{s}^{-1}$. The half life of VEGF-A was instead measured in [187], using a radioactive tracer, giving the value $\tau = 64 \pm 7\,\mathrm{min}$.

Equation (2.6) assumes that cell motion can be obtained on the basis of a suitable force balance. Although the second term in the l.h.s. of the momentum equation reminds us of an inertial term, which is negligible in most biological phenomena, it should be understood instead as a term modelling cell persistence, i.e., the resistance of cells to change their velocity. As a consequence, the r.h.s. implements the reasons which may cause a change in cell directional motion. These include the fundamental chemotactic body force:

$$\mathbf{F}_{chem} = \rho_c \beta(c) \nabla c\,, \tag{2.7}$$

where $\beta(c)$ measures the intensity of the cell response, which can include saturation effects, e.g.

$$\beta(c) = \frac{\beta}{1+\hat{\gamma}c}\,, \qquad \text{or} \qquad \beta(c) = \beta(1-\tilde{\gamma}c)_+\,,$$

where

$$f_+ = \begin{cases} f & \text{if } f > 0\,; \\ 0 & \text{otherwise}\,; \end{cases} \tag{2.8}$$

is the positive part of f. The linear dependence of the force on ρ_c corresponds to the assumption that each cell experiences a similar chemotactic action, so that the momentum balance in integral form depends on the number of cells in the control volume and the related local equation on the local density. The drag force $\mathbf{F}_{cm} = -\epsilon\rho_c\mathbf{v}_c$ was taken to be proportional to the velocity with respect to the substratum and proportional to the cell density for the same reasons as above. Possible generalization of the cell-ECM interaction force should include the mechanisms of integrin attachment and detachment as done in [168].

Finally, the partial stress tensor gives an indication of the response of the ensemble of cells to deformations. Several constitutive equations can be formulated, but unfortunately very little experimental data is available on the mechanical characteristics of cell populations in similar environmental conditions. It can be argued that because the cytosol is a watery solution containing a lot of long proteins contained in a viscoelastic membrane, the ensemble of cells might behave as a viscoelastic material. However, even if one wants to consider such an effect, the characteristic times of the viscoelastic behaviour are much smaller than those related to cell motion (minutes with respect to hours), so that viscoelasticity probably plays a secondary role in the process of vascular network formation. On the other hand, plasticity should probably be taken into account to describe the breaking of cell-to-cell adhesion bonds [13, 168].

In the absence of experimental evidence, the simplest constitutive equation possible,

$$\mathbf{T}_c = -p(\rho_c)\mathbf{I}\,, \tag{2.9}$$

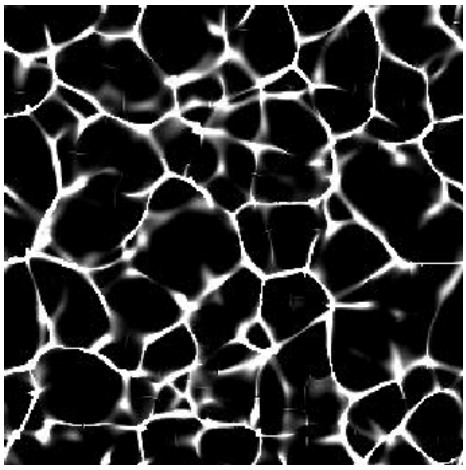

Figure 2: Network structure obtained with the vasculogenesis continuous model (2.4, 2.5, 2.10).

was considered, corresponding to an elastic fluid. This assumption implies, for instance, that the ensemble of cells cannot sustain shear, which, of course, is not true.

Equation (2.6) then specializes to:

$$\frac{\partial \mathbf{v}_c}{\partial t} + \mathbf{v}_c \cdot \nabla \mathbf{v}_c = -\frac{1}{\rho_c} \nabla p(\rho_c) + \beta(c) \nabla c - \epsilon \mathbf{v}_c \,. \tag{2.10}$$

The model (2.4, 2.5, 2.10) can be linked to classical models in particular cases. For instance, dropping both the pressure and the persistence terms in (2.10) corresponds to an immediate adjustment of the cells to the limit velocity and leads to classical chemotactic models (see, for instance, [90, 111, 156]), for which blow-up in finite time is possible under certain conditions. When preserving the pressure term, one has instead the model studied in [106], in which the blow-up of the solution is prevented under suitable conditions on the pressure term, e.g. convexity. Using a Chapman-Eskog expansion, Filbet et al. [62] deduced the above model (2.4–2.6) as a hydrodynamic limit of a kinetic velocity-jump process.

The main feature encoded in the model can be understood in the simplest way by neglecting pressure and assuming for a moment that diffusion is a faster process than pattern formation, so that the time derivative in the diffusion equation can be neglected in a first approximation.

Solving formally the quasi-stationary diffusion equation for c and substituting it in the persistence equation, one can write (for $b = 0$):

$$\frac{\partial \mathbf{v}_c}{\partial t} + \mathbf{v}_c \cdot \nabla \mathbf{v}_c = \frac{a\beta}{D} \nabla \left[\left(\frac{1}{\ell^2} - \nabla^2 \right)^{-1} \rho_c \right] . \tag{2.11}$$

The appearance in the dynamical equations of the characteristic length,

$$\ell := \sqrt{D\tau} \,, \tag{2.12}$$

suggests that the dynamics could favour patterns characterised by this length-scale. As a matter of fact, if we rewrite the right hand side of (2.11) in Fourier space as

$$\frac{a\beta}{D}\,\frac{\mathrm{i}\mathbf{k}}{k^2+\ell^{-2}}\,\rho_{c\mathbf{k}}\,,$$

we observe that the operator $\mathrm{i}\mathbf{k}/\left(k^2+\ell^{-2}\right)$ acts as a filter, which selects the Fourier components of ρ_c having wave numbers of order $1/\ell$ damping the components with higher and smaller wavenumbers. Experimental measurements of the parameters gives $\ell \sim 100\,\mu$m, which is in good agreement with experimental data.

It seems that the process of network formation is then initially driven by the following mechanism: density inhomogeneities are translated in a landscape of concentration of VEGF-A, where details with scale smaller than ℓ fade away. The cellular matter moves by chemotaxis toward the ridges of the concentration landscape, enhancing even further the relevant scale, and eventually producing a network structure characterised by a length-scale of order ℓ. In this way, the model provides a direct link between the range of inter-cellular interactions and the dimensions of the structure, which is a physiologically relevant feature of real vascular networks. The results of a simulation are shown in Figure 2. As expected, changing the diffusion of the chemical factors leads to a change in the typical size of the network, in agreement with the observation that larger effective diffusivities lead to vascular networks with a larger mesh [177].

A detailed analysis on the dependence of the topological characteristics of the structure on the density of seeded cells is then performed in [74, 187]. In a remarkable agreement with the experimental outcomes, they find the percolative and Swiss-cheese transitions described in the previous section, with fractal dimensions consistent with the experimental measurements.

2.1 Exogenous control of vasculogenesis

The generalization of the model to the case of multiple species of chemical factors, characterized by different physical properties and biological actions (e.g., attraction and repulsion) was considered in [109]. The interest in this type of model is due to the possibility of driving for tissue engineering purposes the formation of vascular networks by the use of exogenous chemoattractants and chemorepellents that impregnate suitable gel structures to be disposed on the substratum where the ECs are subsequently plated.

Denoting respectively by c_a and c_r the concentrations of exogenous chemoattrattant and chemorepellent the model in [109] can be written as

$$\frac{\partial \rho_c}{\partial t} + \nabla\cdot(\rho_c \mathbf{v}_c) = 0\,, \tag{2.13}$$

$$\frac{\partial \mathbf{v}_c}{\partial t} + \mathbf{v}_c\cdot\nabla\mathbf{v}_c = -\frac{1}{\rho_c}\nabla p(\rho_c) + \beta(c)\nabla c + \beta_a(c_a)\nabla c_a - \beta_r(c_r)\nabla c_r - \epsilon\mathbf{v}_c\,, \tag{2.14}$$

$$D\nabla^2 c - \frac{c}{\tau} + \alpha\rho_c = 0\,, \tag{2.15}$$

$$D_a\nabla^2 c_a - \frac{c_a}{\tau_a} + s_a(t)H_a(\mathbf{x}) = 0\,, \tag{2.16}$$

$$D_r\nabla^2 c_r - \frac{c_r}{\tau_r} + s_r(t)H_r(\mathbf{x}) = 0\,, \tag{2.17}$$

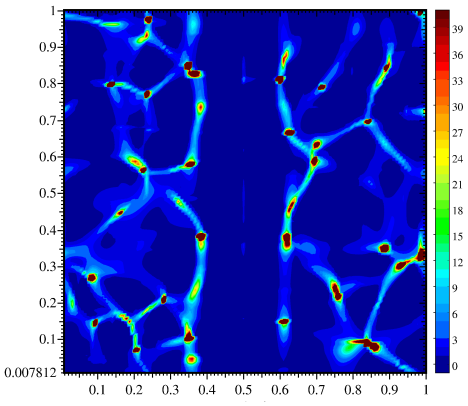

Figure 3: Vasculogenesis simulation in presence of a thin stripe of chemorepellent.

where the time derivatives of the concentrations were dropped because the diffusion characteristic times are much smaller than the one characterizing cell motion. The functions H_a and H_r define where the exogenous chemicals are physically placed while their release is determined by s_a and s_r. For the sake of simplicity, it was assumed that they were constant, which is of course a simplification valid if the release time is much larger than the time of formation of the network, i.e., of the order of ten hours. Of course in some particular cases it may be possible to integrate analytically (2.16) and/or (2.17) so that the relative solution can be directly substituted in (2.14).

In the same way as before, the new diffusion equations (2.16) and (2.17) are characterised by two more natural lengths $\ell_a = \sqrt{D_a \tau_a}$ and $\ell_r = \sqrt{D_r \tau_r}$, related to the ranges of action of the exogenous chemoattractant and chemorepellent, respectively. Within these ranges, the effect of the exogenous chemical factors strongly influence the structure of the network. On the other hand, outside these ranges endogenous chemotaxis governs the formation of a more isotropic network. An example is shown in Figure 3, where a chemorepellent thin stripe is placed in the middle of the figure.

Generally speaking, it was found that the action of chemorepellents is more effective in driving the formation of vascular networks than that of chemoattractants. From the morphological point of view, chemoattractants induce in their range of actions the formation of capillaries which tend to run perpendicularly to their source, while chemorepellent induce the formation of capillaries which tend to run along their source, at a distance of the order of magnitude of their range of action, as shown in Figure 3.

2.2 Substratum interactions

From the phenomenological description in Section 2, it is clear that in a second phase of vascular network formation, the interaction with the substratum and its mechanical properties become important. This is a feature that can not be described by the continuous model proposed above. Indeed, Tosin et al. [208] extended the basic approach (2.4, 2.5, 2.10) by adding in the cell mechanical interactions with the substratum. They still assumed endogenous chemotaxis

only, though the generalization to exogenous chemical factors is straightforward. Though inertial effects can be certainly neglected, releasing the rigidity assumption requires adding a force balance equation for the substratum that can be written as

$$\nabla \cdot \mathbf{T}_m - \mathbf{F}_{cm} + \mathbf{F}_{ext} = \mathbf{0}\,, \tag{2.18}$$

where in particular $\mathbf{F}_{ext}$ is the anchoring force to the Petri dish, that can be taken proportional to the displacement $\mathbf{u}_m$ of the substratum

$$\mathbf{F}_{ext} = -\frac{s}{h}\mathbf{u}_m\,, \tag{2.19}$$

where h is the substratum thickness.

The other interaction force $\mathbf{F}_{cm}$ due to cell-ECM interaction is the one present in the persistence equation (2.6) with the opposite sign as it is an internal force between the two constituents. However, in this case, the deformability of the substratum requires to take into account of the relative motion of the cells with respect to the ECM. In this respect, Tosin et al. [208] assumed that it includes both an elastic and a viscous contribution. During the ameboid motion the interaction force acting on the cells is of viscous type, which implies a weak interaction between the cells and the substratum, characterised by a quick removal of the bonds and formation of new bonds, with weak deformation of the substratum, modelled as

$$\mathbf{F}_{visc} = -\epsilon\rho_c(\mathbf{v}_c - \mathbf{v}_m)\,, \tag{2.20}$$

where $\mathbf{v}_m = d\mathbf{u}_m/dt$.

The elastic contribution takes into account the fact that after some time cells attach to the substratum forming stronger focal adhesion bonds. One can then assume that, if the cell anchors in $\mathbf{u}_m$ and then moves to $\mathbf{u}_c$, then the elastic force is proportional to $\mathbf{u}_m - \mathbf{u}_c$. This change of behaviour characterises the transition between the phase dominated by chemotaxis and that dominated by mechanics. In other words, this force is absent in the initial ameboid motion and starts when the motion becomes of mesenchymal type, i.e. when cells start attaching to the adhesion molecules of the matrigel. In [208] it was assumed that there exists a characteristic time t_{th} needed to anchor to the adhesion sites on the substratum and characterising the transition between a purely ameboid phase and a mesenchymal phase, so that

$$\mathbf{F}_{elast} = -\kappa\rho_c\,(\mathbf{u}_c - \mathbf{u}_m)\,H(t - t_{th})\,, \tag{2.21}$$

where κ is the anchoring rigidity and H is the Heaviside function

$$H(\tau) = \begin{cases} 1 & \text{if } \tau > 0\,; \\ 0 & \text{otherwise.} \end{cases} \tag{2.22}$$

Another interesting hypothesis can be that ameboid motion stops when cells come in contact, so that the strongly reduced velocity allows for a better link with the adhesion molecules of the substratum. This phenomenon could be included in the previous set-up by assuming that

$$\mathbf{F}_{elast} = -\kappa(\rho_c)\rho_c\,(\mathbf{u}_c - \mathbf{u}_m)\,,$$

where in particular $\kappa(\rho_c)$ vanishes below a given value ρ_{th} of cell density, e.g., $\kappa(\rho_c) = \kappa H(\rho_c - \rho_{th})$. This mechanism is consistent with the one involving inter-cellular calcium dynamics described in Section 3.

The model presents a further modification consistent with the above-cited calcium-related dynamics. In fact, the release of endogenous VEGF is assumed to decrease as a consequence of cell-to-cell contact, in agreement with the activation of inhibiting calcium-related pathways described in Section 1.1 and modelled in Section 3. Specifically, it consists in the introduction of a density dependent production of VEGF:

$$\alpha(\rho_c) = \frac{\hat{\alpha}_c \rho_c}{1 + \eta \rho_c^2} \,.$$

In conclusion, considering that while the terms in (2.20, 2.21) must be found in the persistence equation with the opposite sign, the term in (2.19) must not because it does not act on the cellular constituent, the final model can be written as:

$$\frac{\partial \rho_c}{\partial t} + \nabla \cdot (\rho_c \mathbf{v}_c) = 0 \,, \tag{2.23}$$

$$\frac{\partial c}{\partial t} = D \nabla^2 c + \frac{\hat{\alpha}_c \rho_c}{1 + \eta \rho_c^2} - \frac{c}{\tau} \,, \tag{2.24}$$

$$\begin{aligned} \frac{\partial \mathbf{v}_c}{\partial t} + \mathbf{v}_c \cdot \nabla \mathbf{v}_c = &- \frac{1}{\rho_c} \nabla p(\rho_c) + \beta(c) \nabla c \\ &- \epsilon(\mathbf{v}_c - \mathbf{v}_m) - \kappa(\rho_c) \left(\mathbf{u}_c - \mathbf{u}_m\right) \,, \end{aligned} \tag{2.25}$$

$$\begin{aligned} - \frac{E}{2(1+\nu)} \nabla^2 \mathbf{u}_m - \frac{E}{2(1-\nu)} \nabla (\nabla \cdot \mathbf{u}_m) \\ + \epsilon(\mathbf{v}_c - \mathbf{v}_m) + \kappa(\rho_c) \left(\mathbf{u}_c - \mathbf{u}_m\right) - \frac{s}{h} \mathbf{u}_m = \mathbf{0} \,. \end{aligned} \tag{2.26}$$

The effect of mechanical stretching obtained in the simulation is compatible with what is observed in vitro, namely pulling on the extracellular matrix, the cells deform the substratum. However, if the substratum is too rigid or if cell adhesion is too strong, then it is very hard for the cell to form a chord. In the limit of very stiff substrata, then the morphogenic process leads to the formation of lacunae rather than chords, as shown in Figure 4. The mechanical interactions seem also to play an important role in guaranteeing the stability of the network.

3 Cellular Potts Models of Vasculogenesis

Because of the spatial scales involved, cell-based models are particularly suited to catch and describe mechanisms and dynamics mainly occurring at the cell level. In addition, they are more flexible to insert the sub-cellular phenomena of interest, e.g., adhesion mechanisms and activation of protein pathways, into the basic units used to describe the simulated cell.

In this framework vasculogenesis has been widely studied using cellular Potts models (CPM), a lattice-based Monte Carlo technique which follows an energy minimization philosophy [76, 77, 78, 81, 124].

CPM domains dealing with vasculogenic assays use bi-dimensional lattices (i.e., regular numerical repeated graphs). Each grid site $\mathbf{x} \in \Omega \subset \mathbb{R}^2$ is labelled

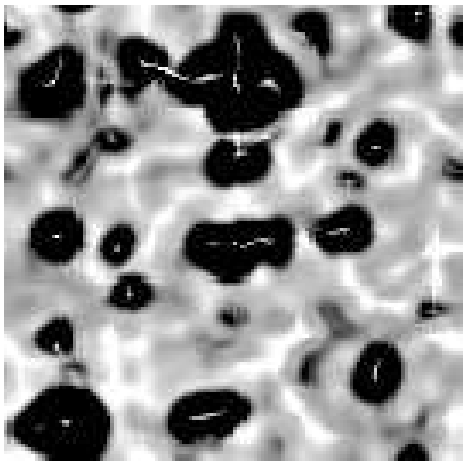

Figure 4: Vasculogenesis simulation in presence of a stiff substratum.

by an integer number, $\sigma(\mathbf{x})$. As typically adopted in CPM models, a neighbour of site $\mathbf{x}$ is identified with $\mathbf{x}'$ while its overall neighbourhood with $\Omega_{\mathbf{x}}^{'}$ (i.e., $\Omega_{\mathbf{x}}^{'} = \{\mathbf{x}' \in \Omega : \mathbf{x}' \text{ is a neighbour of } \mathbf{x}\}$). Sub-domains of contiguous sites with identical spin σ form discrete objects, characterized by an object type, $\tau(\sigma)$.

In classical CPMs of tubulogenesis, each object σ represents an entire and undifferentiated cell, of type $\tau = C$. The experimental matrix substrate (e.g., Matrigel), on which the endothelial cell population resides, is commonly modelled as a generalized object $\sigma = 0$ of type $\tau = M$, assumed to be static, passive and homogeneously distributed throughout the simulation domain, forming no large-scale structures. Connections (links) between neighbouring lattice sites of unlike index $\sigma(\mathbf{x}) \neq \sigma(\mathbf{x}')$ finally represent cell membranes.

As in all CPMs applications, the EC culture gradually and iteratively evolves to reduce a pattern effective energy, given by a hamiltonian H. The functional H contains a variable number of terms, consisting of cell attributes (e.g., volume, surface), true energies (e.g., cell-cell adhesions), and terms mimicking energies (e.g., response to external chemical stimuli). Its local gradient is indeed the "force" acting in any point of the simulation domain. The energy minimization core algorithm is a modified Metropolis method for Monte Carlo dynamics. It is able to implement the natural exploratory behaviour of biological individuals, via thermal membrane fluctuations and biased extensions and retractions of their membranes, with a preference for displacements which reduce the local effective energy of the configuration. To mimic cytoskeletally-driven pseudopod extensions and retractions, a lattice site, $\mathbf{x}_{source}$, is selected at random and assigns its state ($\sigma(\mathbf{x}_{source})$) to one of its unlike neighbours, $\mathbf{x}_{target} \in \Omega_{\mathbf{x}_{source}}^{'}$, which has also been randomly selected. The hamiltonian of the system is computed before and after the proposed update, and the change is accepted with a Boltzmann probability function

$$P(\sigma(\mathbf{x}_{source}) \to \sigma(\mathbf{x}_{target})) = \begin{cases} e^{-\Delta H/T} & \Delta H > 0\,; \\ 1 & \Delta H \leq 0\,, \end{cases} \tag{3.1}$$

where $\Delta H = H_{after\ spin\ flip} - H_{before\ spin\ flip}$ is the net energy difference and T is an effective Boltzmann temperature which in classic CPMs is constant for the

whole system, giving the idea of a generic and homogeneous "culture motility" [129, 130, 131, 132, 133, 183]. A total of n proposed updates, where n is the number of sites of domain Ω, constitutes a Monte Carlo Step (MCS), which is the basic iteration and the unit of time used in the model.

Entering into more detail, in the CPMs of vasculogenesis present in the literature, in [132], the authors use a hamiltonian functional formed by three terms, which control the shape of the ECs, their homotypic (i.e., cell-to-cell) and heterotypic (i.e., cell-ECM) adhesive interactions, and their chemotactic response:

$$H = H_{adhesion} + H_{shape} + H_{chemical}. \tag{3.2}$$

$H_{adhesion}$ phenomenologically implements the general extension of Steinberg's differential adhesion hypothesis (DAH) [81, 191, 192]:

$$H_{adhesion} = \sum_{\mathbf{x}\in\Omega,\mathbf{x}'\in\Omega'_{\mathbf{x}}} J_{\tau(\sigma(\mathbf{x})),\tau(\sigma(\mathbf{x}'))}(1-\delta_{\sigma(\mathbf{x}),\sigma(\mathbf{x}')}), \tag{3.3}$$

where $\mathbf{x}$, $\mathbf{x}'$ represent two neighbouring lattice sites, $\delta_{x,y}$ is the Kronecker delta, and the J's are cell-cell ($J_{C,C}$) or cell-matrix ($J_{C,M}$) binding energies per unit of area. In particular, they are assumed to be constant in time and homogeneous in space.

Instead, H_{shape} imposes on ECs a geometrical constraint. It is written in the following elastic-like form, which increases with the cells deviation from a designated target area A_σ, under the hypothesis that cells do not grow or divide during patterning:

$$H_{shape} = H_{area} = \lambda_C^{area} \sum_\sigma (a_\sigma - A_C)^2, \tag{3.4}$$

where a_σ is the current area of cell σ and λ_C^{area} is an energy penalty (a *Potts coefficient*) representing its resistance to compression.

Finally, for the term $H_{chemical}$, describing the biased walk of ECs up the gradient of VEGF, the authors [181] state that the velocity of the drift depends both on the gradient strength and on the absolute concentration of the chemical, so that the resulting effective-energy change at each copy attempt reads:

$$\Delta H_{chemical} = -(1-\delta_{\sigma(\mathbf{x}_{source}),0})\mu^{ch}\left[\frac{c(\mathbf{x}_{target})}{1+s\ c(\mathbf{x}_{target})} - \frac{c(\mathbf{x}_{source})}{1+s\ c(\mathbf{x}_{source})}\right], \tag{3.5}$$

where s regulates the saturation of the chemotactic response. The chemotaxis coefficient is $\mu^{ch} = \mu^{ch}_{C,M} \gg 0$ at cell-ECM interfaces and $\mu^{ch} = \mu^{ch}_{C,C} = 0$ at cell-cell interfaces, respectively. This ensures that chemotactic extensions occur only at cell-ECM interfaces, reflecting the VE-cadherins suppression of pseudopods (contact-inhibition of chemotaxis). Finally, the factor $(1-\delta_{\sigma(\mathbf{x}_{source}),0})$ is used to implement a pseudopod-extension-only chemotaxis, where only extending pseudopods at the cell-ECM interface respond to the chemoattractant.

Chemoattractant diffusion and degradation is described macroscopically, using a continuum approximation analogous to Eq. (2.5), used in the previously presented models [74, 187]:

$$\frac{\partial c}{\partial t} = D\nabla^2 c + \alpha(1 - \delta_{\sigma(\mathbf{x}),0}) - \epsilon(\delta_{\sigma(\mathbf{x}),0})c(\mathbf{x}, t)\,, \tag{3.6}$$

where α is the secretion rate inside the cells, ϵ the degradation rate in the ECM (i.e., due to proteolytic enzymes or by binding to ECM components), and D the diffusion constant in the ECM, which, although taken slower than that set for VEGF-A165 in [74] and therefore producing steeper gradients, is however sufficient to observe capillary formation.

Such a very interesting model shows that a single set of cell behaviours, i.e., contact-inhibited chemotaxis to an autocrine, secreted chemoattractant, can consistently reproduce the formation of a capillary network in good agreement with the relative *in vitro* experiments, performed with cultures of mouse allantois. The simulations proposed also provide the fact that the pattern emerges over a wide range of cell-cell adhesions and that it is widely independent of cell shape. Moreover, the authors successfully apply the same model to reproduce capillary sprouting from an initially round island of ECs, suggesting common underlying driving mechanisms. In particular, their results show that, at too low cell motilities T, no sprouting occurs if pseudopods responded to the chemoattractant only during extension, as it is necessary to implement an extension-retraction chemotaxis (i.e., by dropping the relative factor in Eq. (3.5)). In contrast, for higher motilities, vascular branching develops with both mechanisms, with a slower process in the case of extension-only chemotaxis. They also investigate how sprouting depends on the chemotactic strength $\mu_{C,M}$: in particular, a critical value separating sprouting from non-sprouting clusters is found. Then, at intermediate values of the parameter, most vascular cords are two cells wide, while for high values the cords become longer and thinner (i.e., only one cell wide). For even higher chemotactic responses, the cells intercalate, moving to the peaks of the chemical gradient. Finally, in order to have a comparison with the model in [74], the authors perform simulations varying the diffusion length of the chemoattractant: in agreement with the continuous approach, they observed that longer diffusion lengths produce thicker cords with larger inter-cord spaces. At the extremes, the clusters do not sprout well when the VEGF diffusion length approaches the EC-cluster diameter, whereas they dissociate if the diffusion length is shorter than the diameter of single cells.

In [131], the same group starts from the experimental observation that endothelial cells dramatically change shape in a second phase of vasculogenesis after cell aggregation. In response to growth factors, intracellular-store-based calcium entry remodels in fact the actin cytoskeletons of ECs, changing their shape from rounded to elongated and bipolar [57] (see also the description in [159]). Such a cell-polarized shape is essential for blood-vessel development. In fact, it causes an anisotropic cell migration, which produces rapidly inter-cellular connections resulting in a fine network, and a sideways movement, which is fundamental for pattern coarsening and stabilization. Therefore, they add to the hamiltonian (3.2), an energetic constraint on cell-length:

$$H_{length} = \lambda_C^{length} \sum_{\sigma} (l_\sigma - L_\sigma)^2, \tag{3.7}$$

where l_σ is the length of cell along its longest axis, L_σ its target length and λ_C^{length} the relative Potts coefficient. In particular, the length of a cell is derived from the largest eigenvalue of their inertia tensor, with the assumption that it

is approximately an ellipse. However, since the length constraint may cause a cell to split into disconnected patches, the authors concomitantly introduce a connectivity constraint, which reflects the physical continuity and cohesion of the actual cell. The rest of this model is analogous with that previously presented, except for the fact that, in this case, the authors do not longer consider a saturation behaviour of the cell chemical response (i.e., they impose $s = 0$ in Eq. (3.5)) and implement a extension-reaction chemotaxis, without contact inhibition (i.e., $\mu^{ch} = \mu^{ch}_{C,M} = \mu^{ch}_{C,C} \gg 0$ in the same equation (3.5)). Interestingly, also with such slightly different assumptions, a standard vasculogenesis process is consistently reproduced, with a final structure resembling a capillary plexus, where cords of cells enclose lacunae homogeneous in dimensions. In this work, the authors also analyse the kinetics of the patterning, finding that the number of branch points and lacunae initially drops quickly, with non-exponential dynamics, then slowly stabilizes, resulting in the typical equilibrium size of the network. Some simulations then show that reducing the target cell length below a critical value (or dropping the length constraint at all) inhibits the formation of the network. Interestingly, by varying the number of simulated cells, these authors find both a percolative and a Swiss-cheese transition analogous to [74].

A more detailed CPM was developed in [105] to reproduce an *in vivo* vasculogenic process during embryonic development, where endothelial precursor cells of mesodermal origin, known as angioblasts, assemble into a characteristic network pattern. In particular, the authors assume that VEGF is not autocrinally produced by the angioblasts, but by the ECM. The EC precursors instead secrete non-diffusive matrix components, able to bind and immobilize the signalling agent in the cell close proximity. Indeed, the authors propose the following system of differential equations for the concentrations of free soluble (c_f) and bound (c_b) VEGF and for ECM molecules (m):

$$\begin{cases} \dfrac{\partial c_f}{\partial t} = D\nabla^2 c_f + \gamma_f - \kappa c_f m - \eta c_f, \\ \dfrac{\partial c_b}{\partial t} = \kappa c_f m, \\ \dfrac{\partial m}{\partial t} = \gamma_m \delta_{\sigma(\mathbf{x}),0} - \alpha c_f m; \end{cases} \tag{3.8}$$

where γ_f and η are the constant rate of VEGF production and degradation, γ_m is the production rate of ECM molecules by cells and the term $\kappa c_f m$ is a mass action with second order kinetics with effective kinetic rate κ.

The system hamiltonian used in such a model is the same as in Eq. (3.2) and takes into account geometrical constraints for angioblasts, homotypic and heterotypic interactions and of the chemical response, which distinguishes between chemotactic cues created by both bound and soluble VEGF:

$$\Delta H_{chemical} = -\mu^{ch}_B(w(\mathbf{x}_{target}) - w(\mathbf{x}_{source})) - \mu^{ch}_S(u(\mathbf{x}_{target}) - u(\mathbf{x}_{source})). \tag{3.9}$$

In particular, the ECM-bound VEGF is assumed to provide a stronger chemical signalling than its freely diffusive forms, as observed in [48, 177], by setting $\mu^{ch}_B > \mu^{ch}_S$.

As demonstrated by a morphometric analysis, this model is able to produce

polygonal cellular patterns that accurately resemble the *in vivo* early vascular bed in quail embryos, recorded by confocal microscopy. The simulated networks show high degree of similarity with respect to a broad spectrum of morphological descriptors, including lacunae number/sizes/shapes, network and interface lengths, cord widths, degree distribution and fractal properties. As observed by the authors themselves, fine-grained spatial cues for chemotactic cell migration can be generated without postulating unrealistically low VEGF diffusion rates [131, 132]. Furthermore, the stability of the network structures increases over time, instead of collapsing after a transient time, as in previous models [74, 131]. Another interesting feature of this work is that cell elongation does not need to be postulated *a priori*, as in [131], as the angioblasts polarize as a natural consequence of chemotaxis towards matrix-bound VEGF. Moreover, a set of simulations reveals two time-scales characterizing the pattern dynamics: in the early stages, a fully connected network forms, whereas, over longer time-scales, it increases in the overall surface area, ensuring an efficient distribution of nutrients and waste removal.

All the CPMs above neglected the evolution of intracellular dynamics that underlie cell phenotypic behaviour. In [184] an extension of CPMs in this direction takes into account specific agonist-induced calcium-dependent pathways that are important to describe the final stabilization phase of the vasculogenic process. In this approach the modelling environment is characterized by a constant flux of information from finer to coarser levels, i.e., the kinetics of the molecular sub-cellular networks strongly determine cell mesoscopic properties and behaviour.

The model specifically referred to tumour-derived endothelial cells (TECs), instead of "normal" endothelial cells, with the relative parameters and protein cascades. Each cell is defined as a compartmentalized unit η, composed of two subregions which, in turn, are standard CPM objects σ: the cell nucleus, a central more or less round cluster of type $\tau = N$ and the surrounding cytosol, of type $\tau = C$. This is obviously a more realistic representation, which allows a more detailed reproduction of cell morphological changes during capillary formation. The TEC population as usual resides in a homogenous matrix, a generalized substrate $\sigma = 0$ of type $\tau = M$.

The hamiltonian of the system is set as

$$H = H_{adhesion} + H_{shape} + H_{chemotaxis} + H_{persistence}. \tag{3.10}$$

$H_{adhesion} = H^{int}_{adhesion} + H^{ext}_{adhesion}$ is similar to the one in Eq. (3.3), but is differentiated in the contributions due to either the generalized contact between subunits belonging to the same cell, or the effective adhesion between membranes of different cells:

$$\begin{aligned} H_{adhesion} = \sum_{\substack{\mathbf{x}\in\Omega \\ \mathbf{x}'\in\Omega'_{\mathbf{x}}}} & \left[J^{int}_{C,N}\delta_{\eta(\sigma(\mathbf{x})),\eta(\sigma(\mathbf{x}'))}(1-\delta_{\eta(\sigma(\mathbf{x})),\eta(\sigma(\mathbf{x}'))}) \right. \\ & \left. + J^{ext}_{C,C}(1-\delta_{\sigma(\mathbf{x}),\sigma(\mathbf{x}')})(1-\delta_{\eta(\sigma(\mathbf{x})),\eta(\sigma(\mathbf{x}'))}) \right]. \end{aligned} \tag{3.11}$$

Here $J^{int}_{C,N} \in \mathbb{R}^-$ is indeed a constant high tension which prevents the cells from fragmenting, whereas $J^{ext}_{C,C}$ represents the local adhesive strength between cells $\eta(\sigma(\mathbf{x}))$ and $\eta(\sigma(\mathbf{x}'))$, whose value will be discussed below.

The geometrical attributes of cell subunits is modelled by

$$\begin{aligned} H_{shape} &= H_{area} + H_{perimeter} \\ &= \sum_{\eta,\sigma} \left[\lambda_{\eta,\sigma}^{area} \left(\frac{a_{\eta,\sigma} - A_{\tau(\sigma)}}{a_{\eta,\sigma}} \right)^2 + \lambda_{\eta,\sigma}^{per} \left(\frac{p_{\eta,\sigma} - P_{\tau(\sigma)}}{p_{\eta,\sigma}} \right)^2 \right], \end{aligned} \tag{3.12}$$

where $a_{\eta,\sigma}$ and $p_{\eta,\sigma}$ are the actual dimensions of the compartments and $A_{\tau(\sigma)}$ and $P_{\tau(\sigma)}$ their target values, which correspond to the typical measures of the nucleus and the cytosol of a TEC in a quiescent state. With respect to the standard formulation (3.4), the form of (3.12) allows finite energetic contributions, as well as a blow-up in the case of $a_{\eta,\sigma}, p_{\eta,\sigma} \to 0$, which means that for instance an infinite energy is needed to shrink a cell to a point. $\lambda_{\eta,\sigma}^{area}$ and $\lambda_{\eta,\sigma}^{per}$ are energy penalties referring to the mechanical moduli of the cell compartments: assuming that TECs do not grow during patterning $\lambda_{\eta,\sigma}^{area}$ is kept high for any η and for σ such that $\tau(\sigma) = C, N$. Moreover, the rigidity of the nucleus is implemented by a high $\lambda_{\eta,\sigma}^{per}$ for any η and for σ such that $\tau(\sigma) = N$. Finally, the elasticity of the cytosolic region, evaluated by $\lambda_{\eta,\sigma}^{per}$ for any η e for $\sigma : \tau(\sigma) = C$, is enhanced by calcium ions, which facilitate cytoskeletal reorganization, as stated below in Eq. (3.16).

$H_{chemotaxis}$ implements an extension-only chemotactic term similar to the one present in [132]:

$$\Delta H_{chemotaxis} = \mu_{\eta}^{ch} \left[Q(\mathbf{x}_{target}) - Q(\mathbf{x}_{source}) \right], \tag{3.13}$$

where, in particular, $\mathbf{x}_{source}$ is a cytosolic site of cell η and $\mathbf{x}_{target}$ is one of its neighbouring medium sites. The quantity

$$Q(\mathbf{x}, t) = \sum_{\mathbf{x}' \in \Omega'_{\mathbf{x}}} c(\mathbf{x}', t), \qquad \text{where} \quad \mathbf{x} \in \{\mathbf{x}_{source}, \mathbf{x}_{target}\},$$

and $\mathbf{x}'$ is a medium first-nearest neighbour of $\mathbf{x}$, evaluates the local extracellular level of VEGF (denoted as usual in this review by c, see Eq. (3.17)) sensed by the moving cell membrane site. μ_{η}^{ch} is the local chemical response of cell η, which is set null at cell-cell interfaces to describe a contact-inhibited chemotaxis.

Finally, $H_{persistence}$ explicitly models the persistent motion characteristic of vascular cells:

$$H_{persistence} = \sum_{\eta} \mu_{\eta}^{pers} |\mathbf{v}_{\eta}(t) - \mathbf{v}_{\eta}(t - \Delta t)|^2, \tag{3.14}$$

where $\mathbf{v}_{\eta}$ is the instantaneous velocity of the center of mass of cell η, and $\Delta t = 1$ MCS. μ_{η}^{pers} controls the cell persistence time and is

$$\mu_{\eta}^{pers} = \mu_{pers,0} \left(\frac{l_{\eta}}{L_0} - 1 \right), \tag{3.15}$$

where $l_{\eta}(t)$ is the current measure of the longer axis of cell η (measured as in [131]), and L_0 is the initial cell diameter. Relation (3.15) describes the fact that, after analogous chemical stimulations, elongated vascular cells have been seen to have a longer persistent movement than round cells [94].

To achieve a more realistic interface between the microscopic, intracellular level and the mesoscopic phenomenological cell scale, in a nested modelling

philosophy in [185] the cell biophysical properties vary as a function of the molecular state, and in particular of the calcium level Ca. Specifically,

$$\begin{cases} J^{ext}_{C,C} = J_0 \ \exp\left(-j\widetilde{Ca}(\mathbf{x},t)\widetilde{Ca}(\mathbf{x}',t)\right) , \\ \mu^{ch}_{\eta} = \mu^{ch}_0 \widetilde{Ca}(\mathbf{x},t) , \\ \lambda^{per}_{\eta,C} = \lambda^{per}_0 e^{-k\widetilde{Ca}_{\eta}(t)} , \end{cases} \tag{3.16}$$

where

$$\widetilde{Ca}(\mathbf{x},t) = \frac{1}{Ca_0} Ca(\mathbf{x},t) - 1 , \qquad \text{and} \qquad \widetilde{Ca}_{\eta}(t) = \frac{1}{a_{\eta}(t) Ca_0} \sum_{\mathbf{x}\in\eta} Ca(\mathbf{x},t) - 1 .$$

These relations mimic the biologically provided fact that the local concentration of calcium ions enhances both the local cadherins' avidity, biologically either with quantitative changes in their expression or with the activation of the already exposed molecules, and the avidity of VEGF surface receptors, whose activity mediates the cell chemotactic force. Moreover, the overall intracellular level of the ion promote continuous and dramatic actin-myosin interactions, resulting in increments in cell elasticity, i.e., in quick changes of cell morphology. Also the motility coefficient T in (3.1) is taken to be an increasing function of the normalized calcium level in the cell $\widetilde{Ca}_{\eta}(t)$.

The constitutive laws summarized in (3.16) represent a step forward with respect to the classical CPMs presented so far; in fact

- Each vascular cell-type features its distinct biophysical properties, which are inherited from its internal molecular state;
- The adhesiveness and the chemotactic strength are no longer homogeneous over the entire cell membrane, but vary locally, revealing the role of microscopic inhomogeneities;
- Cell mesoscopic characteristics are no longer constant over time, but constantly adapt during the process, as a consequence of continuous internal and external stimuli.

The agonist-induced intracellular pathways are approached with a system of reaction-diffusion equations, based on the following set of assumptions:

- VEGF is autocrinally released by TECs, and diffuses and degrades in a finite time throughout the extracellular environment;
- single molecules of morphogen are sequestered by the cells (via their surface tyrosine kinase receptors), and initiate a sequence of reactions culminating in the production of arachidonic acid (AA) and nitric oxide (NO) in the sub plasmamembrane regions [103, 136, 138, 206];
- within cell cytosol NO production is triggered also by AA itself;
- NO and AA open the relative and independent calcium channels in the cell plasmamembrane, leading to extracellular calcium entry [63, 64, 136, 138, 206, 219];

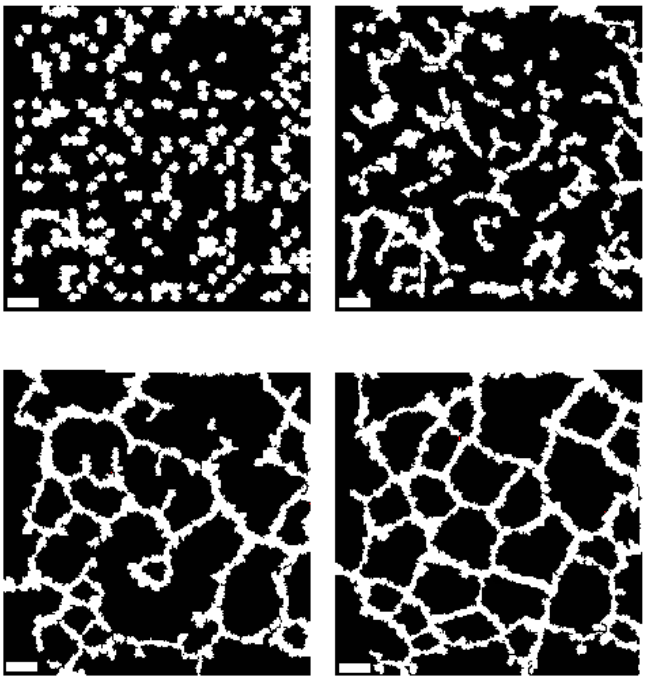

Figure 5: Temporal evolution of the network structure obtained using the cellular Potts model for TEC vasculogenesis ($t = 0, 4, 8, 12\,h$Scale bar=50 μm).

- calcium ions, which also enhance the intracellular production rate of both AA and NO [138], are reversibly buffered to proteins such as calmodulin or to mitochondria [26, 28, 104] and then extruded back from cell by plasmamembrane calcium ATPase and Ca^{2+}-Na^{+} exchangers [80, 93, 213].

Indeed, the extracellular evolution of VEGF (always denoted by c) is controlled by:

$$\frac{\partial c}{\partial t} = D_c \nabla^2 c - \frac{c}{\tau} - B(c) + S\,, \tag{3.17}$$

where $S = S(\mathbf{x}, t)$ describes the autocrine secretion of the growth factor from cells' membrane at a constant rate. VEGF binding and uptake by tumour-derived ECs defined by $B(c)$ is proportional to the local concentration of the ion and is limited to a maximum rate related to the number of membrane receptors.

For each cell η, the current local levels of AA and NO (i.e., at site $\mathbf{x}$: $\tau(\sigma(\mathbf{x})) = C, N$) are defined, respectively, as $a(\mathbf{x}, t)$ and $n(\mathbf{x}, t)$, and are controlled by the following diffusion equations [142, 184, 185]:

$$\frac{\partial a}{\partial t} = D_a \nabla^2 a - \frac{a}{\tau_a} + \gamma_a R(B(c)) + \tilde{\gamma}_a Ca\,, \tag{3.18}$$

$$\frac{\partial n}{\partial t} = D_n \nabla^2 n - \frac{n}{\tau_n} + \gamma_n R(B(c)) + \tilde{\gamma}_n \frac{Ca}{s_n + Ca}\,\frac{a}{s_a + a}\,. \tag{3.19}$$

The third terms in Eqs. (3.18) and (3.19) describe the production rate of AA and NO at the cells' membrane, which are proportional to the quantity of

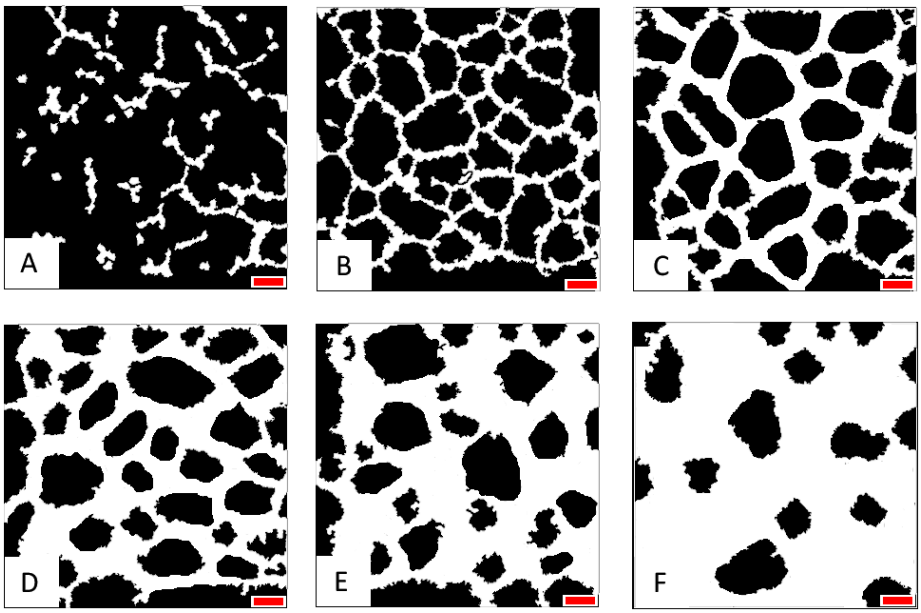

Figure 6: Dependence of the CPM model for TEC vasculogenesis on the density of seeded cells ($n = 50, 150, 200, 300, 400, 500$. Scale bar=50 μm).

sequestrated VEGF molecules (i.e., B is defined as in (3.17)). The last term in Eq. (3.18) implements the calcium-dependent feedback mechanism in AA bio-synthesis, while the analogous term in Eq. (3.19) accounts for the double regulation of NO production (both AA- and Ca-mediated).

For each cell η, the intracellular concentration of calcium, defined as $Ca(\mathbf{x}, t)$, is controlled by the following reaction-diffusion equation:

$$\begin{cases} \dfrac{\partial Ca}{\partial t} = K_{buff} D_{ca} \nabla^2 Ca, & \text{in } \eta; \\ \mathbf{n} \cdot \nabla Ca = k_{Ca}(Ca - \widehat{Ca})_+ \dfrac{k_a a}{q_a + a} + \dfrac{k_n n}{q_n + n}, & \text{at the boundary of } \eta, \end{cases} \tag{3.20}$$

where the scaling factor $K_{buff} < 1$ models the activity of intracellular endogenous buffers, which decreases the intracellular diffusion of calcium.

As shown in Figure 5, the resulting model is able to describe a TEC tubulogenic assay, with a number of parameters which are under control and biologically significant. Indeed, it yields a close dependence of the topology of the structure on cell density, as that observed in [74, 131] for normal ECs (see Figure 6).

The activation/inactivation of calcium dynamics is evidenced in Figure 7. In particular, calcium related networks are up-regulated during the migration phase and switch off upon reaching confluence leading to a decrease in motility.

The connection between cell-based models with the sub-cellular chemical machinery allows to virtually test specific and biologically reasonable anti-angiogenic strategies, which produce an abnormal capillary-like bed. In particular, reviewing the results (see Fig. 8), the proposed model confirms the efficiency of current therapies, which focus on the abrogation of VEGF activity or with

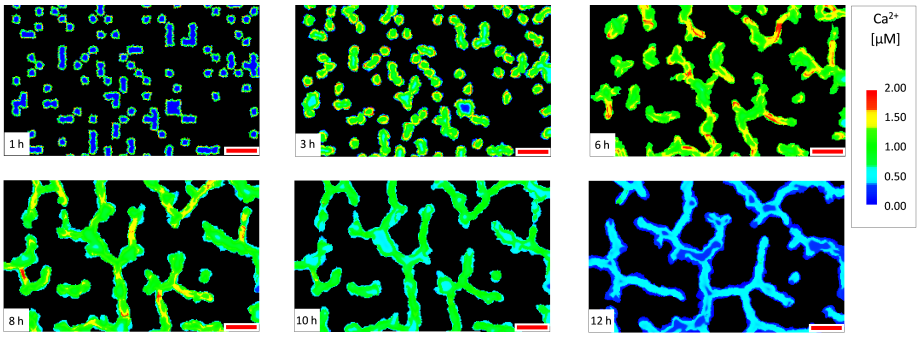

Figure 7: Temporal evolution of calcium within ECs involved in tubule formation.

the interference with calcium machinery, and can suggest novel and interesting cancer therapies, e.g., blocking the mechanisms of cytoskeletal remodelling and inter-cellular adhesion or inhibiting the chemotactic and persistent component of cell motion. All of the proposed solutions indeed emerge by opportune and biologically reasonable variations in model parameters or assumptions.

For sake of completeness, we mention the papers by Szabo et al. [201, 202], who instead used an individual cell-based model to describe vasculogenesis.

4 Angiogenesis

Though angiogenesis is a physiological process occurring, for instance, in wound healing, ovary and uterus vascularization during the female cycle, mammary gland vascularization during lactation, most of the literature on angiogenesis focuses on tumour-induced angiogenesis, one of the most dangerous pathological aspects. In fact, one of the crucial milestones in tumour development is the so-called angiogenic switch, i.e., the achieved ability of the tumour to trigger the formation of its own vascular network by the secretion of angiogenic factors.

As expected angiogenesis has many similarities with vasculogenesis, though the origin is very different. In fact, in this case the new vessels sprout from existing capillaries and post-capillary venules. Angiogenesis is regulated by precise genetic programmes and is strongly influenced by many chemical factors generally called tumour angiogenic factors (TAF) and the subsequent activation of even more related pathways. Some of the proteins involved are vascular endothelial growth factor (VEGF), transforming growth factor β (TGF-β), basic fibroblast growth factor (bFGF), hypoxic growth factor (HIF), platelet-derived growth factor (PDGF), metallo-proteinases (MMP), angiopoietin (Ang). In addition, there are several cell populations influencing the process, e.g., through inflammation and vessel maturation, like macrophages, pericytes, smooth muscle cells. All this makes the process very complex and the interested reader can find more information for instance in [15, 39, 43, 44, 123].

The first stage of angiogenesis is characterized by changes in the shape of ECs covering the walls of the blood vessel, by the loosening of the adhesive connection between cells, and by the reduction of vascular tonus. This in particular induces an increase in the vessel permeability which results as a first consequence in an

OPTIMAL POTENTIAL THERAPIES				
BIOLOGICAL MECHANISM	**MODEL PARAMETER**	**EFFICIENCY**	**EXISTING COMPOUND**	**TOTAL TUBULE LENGTH (μm)**
VEGF UPTAKE	β_V	+++	sorafenib, sunitinib, vatalanib	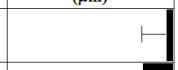
VEGF DEGRADATION	λ_V	+++		
CALCIUM ENTRY	F_{AA}, F_{NO}	+++	CAI	
AA PRODUCTION	v_{AA}, c_{AA}	+	AACOCF3	
NO PRODUCTION	$v_{Ca\text{-}AA}$, v_{NO}	+	L-NAME, L-NMMA	
CYTOSKELETAL REMODELING	μ_{pers}	+++	phalloidin	
PERSISTENCE	μ_{in}	+++		
CHEMOTAXIS	μ_{ch}	+++		
ADHESION	$J^{ext}(C,C)$	+++	anti-VE-cadherin antibodies	
CONTROL				

Figure 8: Potential anti-angiogenic therapies. Each line represents a possible strategy to inhibit the VEGF-induced tubulogenesis. The relative modified parameters are given in the second column. Third column gives an idea of the efficiency of the proposed solutions: +++ means a reduction larger than 66%, ++ in the range 50% – 66% and + in the range 33% – 50% in total tubule length with respect to the physiological value. The last column report the relative average values (mean over 10 simulations, error bars show standard deviation).

increase in the availability of nutrients and in the interstitial pressure.

The following step consists in the production of proteolytic enzymes (serine-proteins, iron-proteins) which degrade the basal lamina and the extracellular matrix surrounding the capillary facilitating the cellular movement. ECs acquire then the possibility to proliferate and to migrate chemotactically toward the place where it is necessary to create a new vascular network. In this phase it is possible to distinguish between tip cells leading the way through the ECM and stalk cells forming in the rear of the lumen of the new capillary. During growth, capillaries may branch or merge to form loops when two capillaries encounter, a process called anastomosis. From these branches and loops more sprouts may form. Indeed, the whole process may repeat several times forming a capillary network through which blood may circulate.

The stage of differentiation is characterized by the exit of ECs from the cellular cycle and by their capacity of surviving in sub-optimal conditions and of building themselves primitive capillary structures, not yet physiologically active. Finally, in the stage of maturation, the newborn vessel is completed by the formation of new perivascular ECM and by the arrival of pericytes and sometimes of flat muscle cells. During this phase a major role is played by angiopoietins (Ang-1, Ang-2) leading to the development of the simple endothelial tubes into more elaborate vascular tree composed of several cell types. In fact, they contribute to the maintenance of vessel integrity through the establishment of appropriate cell-cell and cell-matrix connections.

After the formation of the vascular network, a remodelling process starts influenced by the blood flow. This involves the loss of some physiologically useless capillaries, adaptation of the size of the lumen, and remodelling of the extracellular matrix.

Angiogenesis can also be simulated in vitro [16, 68] as clusters of ECs are able to migrate, to proliferate and to build structures which are similar to capillaries when cultivated in extracellular matrix gel.

For sake of completeness a further process leading to vessel formation is arteriogenesis, a process triggered by the occlusion of an artery. In order to overcome the problems of possible formation of ischemic tissues, the pre-existing arteriolar connections enlarge to become true collateral arteries. In this way, bypassing the site of occlusion, they have the ability to markedly grow and increase their lumen providing an enhanced perfusion to regions interested by the occlusion. It has to be remarked that the formation of collateral arteries is not simply a process of passive dilatation, but of active proliferation and remodelling. However, no model has devoted attention to this process.

5 Hybrid Models of Angiogenesis

The first angiogenesis model was proposed in [21] followed by many others (see, for instance, [40, 53, 91, 92, 96, 112, 113, 114, 115, 154, 163, 180, 190]). However, at variance with the vasculogenesis models discussed above, in these approaches the use of fully continuum approaches did not allow to capture the morphology of the capillary networks. An exception is the model by Travasso et al. [210]

that can be written as follows:

$$\frac{\partial \rho_s}{\partial t} = K\nabla^2\left(\rho_s^3 - \rho_s - \epsilon\nabla^2\rho_s\right) + \gamma_s \min\{c, c_{max}\}\rho_s\,, \tag{5.1}$$

$$\frac{\partial c}{\partial t} = \nabla\cdot(D\nabla c) - \delta_c\rho_c + \alpha(\omega)\,, \tag{5.2}$$

where ρ_s represents the density of stalk cells, c the angiogenic factors, K is the motility coefficient, ϵ is the width of the capillary wall, δ_c is the uptake coefficients from ECs and a random source of TAF $\alpha(\omega)$ is placed in the system. Finally, the tip cells, not clearly connected with the rest of the system, move chemotactically with velocity:

$$\mathbf{v} = \beta \min\{|\nabla c|, G_{max}\}\frac{\nabla c}{|\nabla c|}\,, \tag{5.3}$$

where β is the chemotactic response of tip cells, and G_{max} is a saturation coefficient. The term in the laplacian in (5.2) destabilizes solutions with small ρ_s, giving rise to a backward heat equation term that is however stabilized by the bilaplacian. This results in an aggregation-like mechanism, well known in phase field theory and sometimed denoted as spinoidal decomposition, that can be found in other tumour growth models (see, for instance, [47, 227]).

Actually, in (5.2) the growth term in the first equation and the reaction term in the second equation are put to zero when the density becomes negative, a situation that a proper numerical integration of the model should not allow. The final result is a branching structure aiming at the chemotactic source similar to vascular trees.

The breakthrough in modelling realistic vascular structures was represented by the idea proposed by Anderson and Chaplain [14] consisting essentially of the following: instead of using reinforced random walk methods to obtain a continuous model from a discrete one, let's keep the discrete feature for the capillary sprout tip cells, following their random path toward the tumour, or even let's go back to a discrete and stochastic version of a continuous model to catch the cell-scale structures (see also [15, 164, 165, 166, 188]). Focussing on the ECs at the sprout-tips, where in the absence of branching there is no proliferation, the basic model is written as:

$$\frac{\partial \rho_c}{\partial t} + \nabla\cdot\left[\left(\beta(c)\nabla c + w_f\nabla f\right)\rho_c\right] = k_\rho\nabla^2\rho_c\,, \tag{5.4}$$

$$\frac{\partial c}{\partial t} = -\delta_c n c\,, \tag{5.5}$$

$$\frac{\partial f}{\partial t} = \gamma n - \delta_f n f\,, \tag{5.6}$$

where ρ_c is the density of ECs, f is the concentration of fibronectin, δ_c is the uptake coefficients from ECs, δ_f is the degradation of fibronectin and γ is the production rate of fibronectin by the cells.

Therefore, the TAF secreted by the tumour diffuses into the surrounding tissue and sets up the initial concentration gradient between the tumour and any pre-existing vasculature, which is responsible for the directionality in the formation of the new capillaries. Later on, endothelial cells uptake TAF. However, diffusion is neglected.

As mentioned above, the main idea consists in using the resulting coefficients of the five-point stencil of the standard central finite-difference scheme to generate the probabilities of movement of an individual cell in response to the chemoattractant gradients and to diffusion.

Working in 2D, if P_0 is related to the probability of the cell of being stationary and to the probability of cells of moving away from the node $\{i, j\}$ to one of its neighbours, P_1 is related to the probability of new cells coming from the node to the right, and similarly for the others, one can write

$$\rho_{j,k}^{i+1} = P_0\rho_{j,k}^i + P_1\rho_{j+1,k}^i + P_2\rho_{j-1,k}^i + P_3\rho_{j,k+1}^i + P_4\rho_{j,k-1}^i\,,$$

$$c_{j,k}^{i+1} = \left(1 - \Delta t\delta_c\rho_{j,k}^i\right) c_{j,k}^i\,,$$

$$f_{j,k}^{i+1} = \left(1 - \Delta t\delta_f\rho_{j,k}^i\right) f_{j,k}^i - \Delta t\gamma\rho_{j,k}^i\,,$$

where, for instance,

$$\begin{aligned}
P_0 &= 1 - \frac{4\Delta t k_\rho}{\Delta x^2} \\
&\quad + \frac{\Delta t}{4\Delta x^2}\,\frac{\beta_0 c_M}{(c_M + c_{j,k}^i)^2}\left[(c_{j+1,k}^i - c_{j-1,k}^i)^2 + (c_{j,k+1}^i + c_{j,k-1}^i)^2\right] \\
&\quad - \frac{\Delta t}{\Delta x^2}\left[\frac{\beta_0 c_M}{c_M + c_{j,k}^i}\left(c_{j+1,k}^i + c_{j-1,k}^i + c_{j,k+1}^i + c_{j,k-1}^i - 4c_{j,k}^i\right)\right. \\
&\qquad \left. + w_f\left(f_{j+1,k}^i + f_{j-1,k}^i + f_{j,k+1}^i + f_{j,k-1}^i - 4f_{j,k}^i\right)\right], \\
P_1 &= \frac{\Delta t k_\rho}{\Delta x^2} - \frac{\Delta t}{4\Delta x^2}\left[\frac{\beta_0 c_M}{c_M + c_{j,k}^i}(c_{j+1,k}^i - c_{j-1,k}^i) + w_f(f_{j+1,k}^i - f_{j-1,k}^i)\right].
\end{aligned}$$

In particular, if there is no chemical gradient, the situation is isotropic and the probabilities $P_1, \ldots, P_4$ of moving in any direction are equal. Even in this case, the extraction of a random number will decide whether the tip cell will stay still or will move to a particular neighbouring node rather than another. On the other hand, in presence of a chemical gradient the random walk becomes biased, because the cell has higher probabilities to move up the gradients of chemical factors.

In addition to that, the discretized set-up allows to include some phenomena that are difficult to describe using a model based on partial differential equations, e.g., capillary *branching* and *anastomosis* leading to the formation of capillary loops. In particular, they assumed that the density of endothelial cells necessary to allow capillary branching is inversely proportional to the distance from the tumour and proportional to the concentration of TAF. However, a minimal distance from the previous branching point is needed for a further ramification, and of course. there must be enough space in the discretized space to allow the formation of a new capillary. This assumption is consistent with the observation that the distance between successive branches along the capillaries decreases when the tumour is approached. This phenomenon is called *brush border effect* and is well described by the model and the simulation. In this

approach it is even easier to describe anastomosis. When during their motion a capillary tip meets another capillary, then they merge to form a loop. If two sprout tips meet, then only one of the original sprouts continues to grow.

This modelling approach, developed for tumour angiogenesis, has also been applied to wound healing [118, 198] and to retinal angiogenesis [19, 207, 220]. Other developments more directed to better numerical implementation and visualization can then be found in [116, 134, 197, 203, 204, 225], yielding very realistic vascular structures (see also the three-dimensional animation available at the web site www.maths.dundee.ac.uk/šanderso/3d/index.html).

In principle, the method would easily allow to include a dependence of the chemotactic sensitivity, of the proteolytic activity and after all of the probabilities of motion and branching from the activation of proper protein networks. However, to our knowledge the problem has not been addressed yet.

Capasso and Morale [42] instead modelled the branching mechanism as a stochastic marked counting process. The network of vessels is modelled as the union of the trajectories developed by tip cells, according to a system of Langevin-like stochastic differential equations.

The model in [21] was then used and modified to include blood flow in the capillary network and consequent vessel remodelling [126, 127, 193, 194, 230] and also pericyte recruitment [128] (see also the review [46]). In more detail, the capillary network is treated as a series of straight small tubes in which blood flows according to a fully developed Poiseuille flow. In this way in each capillary the flow Q is related to the pressure drop ΔP between the extrema of the straight cylinder through the classical expression:

$$Q = \frac{\pi R^4 \Delta P}{8 \mu_{app} L}\,, \tag{5.7}$$

where R and L are respectively the radius and the length of the capillary branch and μ_{app} is the apparent (or effective) blood viscosity. In fact, as well known, blood is a complex biphasic mixture of cells and plasma, certainly possessing viscoelastic characteristics. The relative effect of the cellular constituent depends on the width of the capillary in a very complex manner. Pries and Secomb [169] tried to overcome the problem by proposing the following experimental fit for the apparent or effective viscosity of blood:

$$\mu_{app}(R, H_D) = \mu_{plasma}\left[1 + (\mu_{0.45}(R) - 1) f(H_D) g(R)\right] g(R)\,, \tag{5.8}$$

where H_D discharge hematocrit (normally $H_D = 0.45$) and

$$f(H_D) = \frac{(1 - H_D)^n - 1}{(1 - 0.45)^n - 1}\,, \tag{5.9}$$

$$g(R) = \left(\frac{2R}{2R - 1.1}\right)^2\,, \tag{5.10}$$

$$\mu_{0.45} = 3.2 + 6e^{-0.17R} - 2.44e^{-0.06(2R)^0.0645}\,, \tag{5.11}$$

$$n = \left(0.8 + e^{-0.15R}\right)\left(\frac{1}{1 + 10^{-11}(2R)^{12}} - 1\right) + \frac{1}{1 + 10^{-11}(2R)^{12}} \tag{5.12}$$

Kirchhoff's law then holds at the capillary junctions to describe the mass distribution.

One of the main aims of the above developments is to use the outcome of the vascular network model to study drug perfusion. For instance, it was found that a rather irregular and highly connected network led to poor blood flow to the tumour and therefore poor drug delivery.

Referring again to the results by Pries and Secomb [170, 171, 172, 173, 174], the model for vessel adaptation and remodelling is the following:

$$\frac{1}{R}\frac{dR}{dt} = \log(\tau_w(Q) + \tau_{ref}) - k_p \log \tau_e(P) + k_m \log\left(\frac{Q_{ref}}{QH_D} + 1\right) - k_s\,, \quad (5.13)$$

where the first term refers to the effect of wall shear stress:

$$\tau_w = \frac{4\mu_{app}|Q|}{\pi R^3}\,, \quad (5.14)$$

and τ_{ref} is a small constant included to avoid singularities at low shear rates; the second term refers to the effect of intravascular pressure measured in millimetres of mercury:

$$\tau_e(P) = 100 - 86\exp\left[-5000[\log(\log P)]^{5.4}\right]\,; \quad (5.15)$$

the third term refers to the effect of metabolic hematocrit; and the last to the natural shrinking tendency of capillaries.

In [119, 231] the hybrid approach described above was then coupled with a tumour growth model previously deduced in Cristini et al. [51] then applied to tumour cell invasion [70] and to vascular growth of gliomas in particular [27].

The same purpose was pursued by Alarcon and co-workers [4, 5, 6, 7, 8, 33, 41, 157], who used a cellular automata model. The hybrid characteristic is mantained as nutrients and chemical factors, mainly VEGF, evolve according to diffusion equations, suitably discretized using a finite difference scheme. Subcellular models of the cell cycle govern cell proliferation and apoptosis through the activation of p53. The underlying vasculature permeating the tissue that presents some tumour cells developing in a vascularized tumour mass is a preexistent network with an hexagonal structure. In more detail, vascular remodelling is considered in [7, 41] keeping the network structure, i.e., without new vessel sprouting from the original network, but adjusting the size of the capillaries with time according to the rules proposed by Pries and Secomb recalled in Eq. (5.13). Following the ideas in [79, 97, 98], in [7] the model is further developed to focus on vessel normalisation in view of the optimisation of drug delivery. In [157] the vessel network evolves via sprouting of tip cells with a probability that increases with the local VEGF concentration and anastomosis forming new capillary loops, and pruning in the case of vessel segments with low wall shear stress.

Perfahl et al. [162] extended the model of Owen et al. [Al23] to three spatial dimensions. Each lattice site can be occupied by several cells that can move according to a reinforced random walk. The ensemble of cells is superimposed onto a vascular network consisting of vessel segments connecting adjacent nodes on the lattice. As initial conditions they used an experimentally derived vascular network and tried to predict the outcome of the in vivo experiment. Nutrients and chemical factors perfuse in and out of the network. The vessel network evolves again via sprouting, anastomosis and pruning. An example of simulation is given in Figure 9.

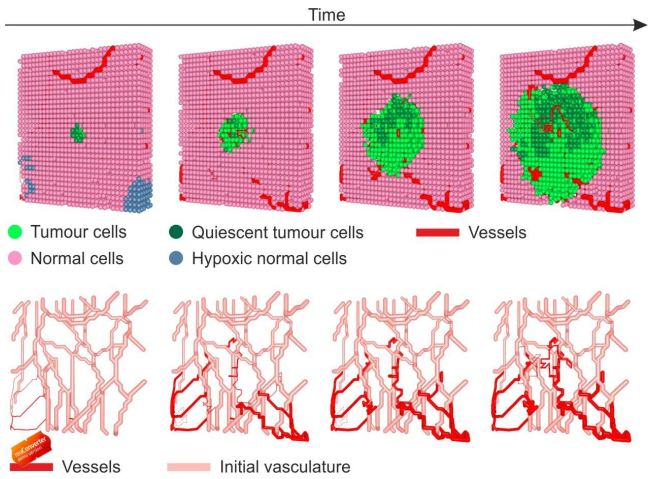

Figure 9: Angiogenesis model joined with a tumour growth model as simulated by the model presented in [162]. By courtesy of H. Perfahl.

Gevertz and Torquato [75] study angiogenesis and vascular growth of glioblastoma using a cellular automata model based on a Voronoi tessellation. Tumour cells are divided into proliferative cells, non-proliferative/hypoxic cells, and necrotic cells. The tissue is provided with a capillary network with a honeycomb structure as in [23, 222, 223, 224] discussed below. The network then evolves according to the production and diffusion of several proteins such as VEGF and angiopoietins, and according to the presence of the related receptors.

Another cellular automaton model not coupled with tumour growth was proposed in [125]. In this article, the authors focused more on the mechanisms underlying isotropic morphogenesis, including dichotomous and lateral branching, blind vessel ends, and closed loops due to anastosmosis, lateral inhibition of an autocatalytic morphogen, as well as a genetic switch that differentiates tissue into substrate-depleting vessels.

In a similar way, still considering vessel remodelling, dilation, pruning, sprouting, and tip cell movement described by a reinforced random walk, Reiger and co-workers discretized the vascular network on a more dynamic cubic lattice [23] and then in an hexagonal lattice [222], then focusing on arterio-venous sytems [223] also including the dynamics occurring at the cell level involving vessel wall degradation or maturation [224].

Finally, a cellular Potts model like the one described in Section 3 is used in [24, 25] to describe angiogenesis in a 2D environment filled with fibers of ECM cleaved by the action of the tip cells. The evolution of chemical factors is again linked to proper reaction-diffusion equations.

Drasdo et al. in [59] embedded a tumour in a network of capillaries with a cubic symmetry. The ensemble of cells was described by his well-known individual cell-based model (see, for instance, [58]) while the capillary network was allowed to undergo angiogenesis.

For sake of completeness we also mention the articles by Astanin and coworkers [17, 18] and Bertuzzi and co-workers [29, 30, 31, 32], who used PDE

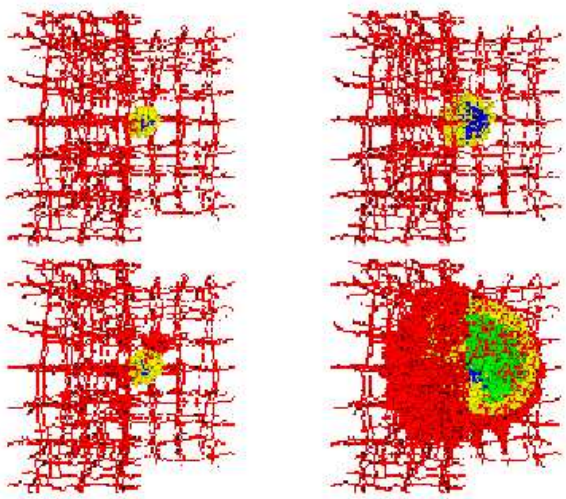

Figure 10: Tumour growth as simulated by the individual cell-based model presented in [59] in a static vessel network (left) and with angiogenesis (right). By courtesy of N. Jagiella (modified from [59]).

models to describe growth of tumour cords along pre-existing capillaries and capillary networks (see Figure 11) but without angiogenesis.

A different issue related to tumour-induced angiogenesis was studied by Addison-Smith et al. [3] who focused on the mechanisms of sprout formation. In fact, in the previous models, the initial point of the sprout on the existing capillary was either given a priori or determined stochastically. Instead Addison-Smith et al. [3] developed a simple mathematical model to determine the probable locations of the sprouts and the relative inter-distance.

6 Lymphangiogenesis

The lymphatic system plays a key role in the human body because it forms the main tissue-drainage system, thus helping to maintain tissue-fluid homeostasis [199]. Its primary function is to keep and control a pressure gradient from blood capillaries through the interstitium to the lymphatic vessels, to allow the clearance of extravasated fluids, tissue waste products, and plasma proteins, but it is also involved in fat metabolism and in graft rejection. It is also well-known that the lymphatic system is essential for immuno-surveillance in the body, since it provides one of the main routes for the immune cells. So it is not difficult to understand that a malfunctional lymphatic system may lead or contribute to many diseases, such as lymphedema, fat metabolism, immune diseases, psoriasis, Melkersson-Rosenthal-Meischer syndrome, Kaposi sarcoma, lymphatic filariasis, Crohn's disease, and chronic inflammation in general [9, 102, 160].

In addition, the lymphatic network plays a relevant role in cancer dynamics. On the one hand, cancer cells usually intravasate the lymph vessels to metastasize the cancer in the body, and there are also indications that tumour lymphangiogenesis is correlated with cancer metastasis (see, for instance,

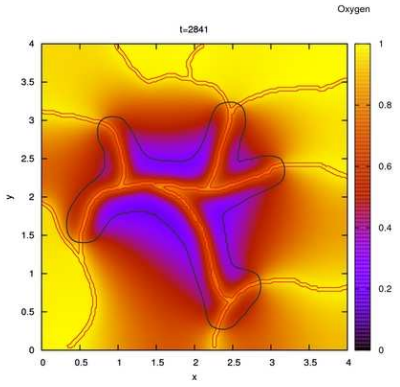

Figure 11: Growth of a tumour cord in a vascular network. Colours indicate the concentration of oxygen. It is possible to notice how the increased metabolism of tumour cells leads to the formation of a hypoxic region away from the capillaries.

[1, 55, 120, 189, 200]). On the other hand, a malfunctional lymphatic system leads to an increase in interstitial pressure leading to a swollen tissue and a difficulty in drug delivery [97, 98]. In addition, a reduction in the pressure gradient in the tissue between the blood and the lymphatic system leads to a much slower, mainly diffusive, movement of nutrients and thus to an increased accumulation of waste products in the tissue.

The term lymphangiogenesis is used to refer to the development of lymphatic vessel networks both *de novo* and from pre-existing networks. However, in spite of the evident importance, lymphangiogenesis is much less studied than angiogenesis and vasculogenesis, and the morphological, spatial, and temporal features of lymphangiogenesis are poorly understood. A recent review of *in vitro* and *in vivo* experimental models for investigating lymphangiogenesis can be found in Bruyère and Noël [35]. Previously, research was hindered by the lack of markers for the lymphatic vessels, but this has been remedied in the last couple of decades by the identification of specific molecular markers, such as Prox1 (transcription factor), podoplanin (transmembrane glycoprotein), LYVE-1 (lymphatic vessel hyaluronan receptor 1) and VEGFR-3 (vascular endothelial growth factor receptor-3) [52].

The formation of lymphatic networks is coordinated primarily by the growth factors VEGF-C and VEGF-D, mediated through the receptor VEGFR-3 [20]. VEGF-C, in particular, appears to be the most essential factor in promoting lymphangiogenesis by generating a chemotactic response from the lymphatic endothelial cells (LECs). This process differs from angiogenesis and vasculogenesis of blood endothelial cells, which is mainly induced by VEGF-A, and mediated through the receptor VEGFR-2; see [178, 205] for excellent illustrations of the molecular characteristics of blood and lymphatic endothelial cells, and [2, 101, 153] for further information on the molecular biology of lymphangiogenesis. Other influences on lymphatic network development come from the molecular interactions between the LECs and their local ECM biophysical and

molecular environment, which can affect migration, adhesion, proliferation, differentiation and organisation [100, 226].

Starting from the observation that one of the main roles of the lymphatic system is to maintain interstitial fluid balance and protein convection, Swartz and co-workers [34, 66, 87, 88, 152] have investigated the effects of interstitial flow on lymphangiogenesis. In [34], they observed *in vivo* that interstitial fluid channels formed in a collagen implant before LEC organization, and lymphatic capillary network organization was initiated primarily in the direction of lymph flow. Subsequently, they have shown *in vitro* that blood and LEC morphogenesis is triggered differentially by very low rates of interstitial flow [152], and by the synergistic combination of interstitial flow and proteolytic release of ECM-bound VEGF, [87]. In the latter case, they accounted for the synergy by proposing, and demonstrating with the support of an advection-diffusion model, that the flow generates a downstream bias in the distribution of VEGF and a shift in the maximum concentration, that the cell will follow like a carrot constantly held in front of the cell's head (see also [66], where this phenomenon is described as the generation of "autologous morphogen gradients"). The work was then extended to explore the effects of ECM composition on the endothelial cell reorganisation [88] by manufacturing matrices with different proportions of fibrin and collagen. They found that organisation of blood and LECs preferred distinct matrix compositions, and that the structures produced were morphologically different.

Compared to angiogenesis and vasculogenesis, very little has been done also on modelling the formation and remodelling of lymphatic vessels. To explain the collagen pre-patterning caused by interstitial fluid flow before the migration of LECs to form networks observed in [34], Roose and Fowler [176] proposed a model developed in the framework of the theory of mixtures and using the theory of two phase rubber materials due to Flory and coworkers [67]. The model considers the interaction of the collagen gel with a solute, such as protons, which can remodel the gel. It consists of two coupled fourth order partial differential equations describing the evolution of the collagen volume fraction ϕ and the solute concentration c, that can be written as follows

$$\frac{\partial \phi}{\partial t} = \nabla \cdot \left\{ \phi^2 (1-\phi)^2 \left[F \nabla \phi - \kappa \nabla (\nabla^2 \phi) + G \nabla c \right] \right\} , \tag{6.1}$$

$$\begin{aligned} \frac{\partial c}{\partial t} = \nabla \cdot \left\{ -c\phi^2 (1-\phi)^2 \left[F \nabla \phi - \kappa \nabla (\nabla^2 \phi) + G \nabla c \right] \right\} \\ + \frac{1}{Pe} \nabla \cdot \left[D(\phi) \nabla c \right] , \end{aligned} \tag{6.2}$$

where Pe is the Peclet number. Here $F = f_{\phi\phi} - c f_{\phi c}$ and $G = f_{\phi c} - c f_{cc}$, where the function f measures the influence of entropy, enthalpy and elastic energy on the organisation of the collagen gel, and is given by:

$$f = (1-\phi)\log(1-\phi) + \chi\phi(1-\phi) + \frac{1}{2N_x}\left(\phi_0 - \phi - \frac{1}{3}\phi \log \frac{\phi_0}{\phi} \right). \tag{6.3}$$

As the sign of the terms F and G is not determined, there might be an anti-diffusive term in the equation for the volume fraction (6.2), though regularized by the bi-Laplacian, as in the angiogenesis model in [210]. They studied the linear stability of the homogeneous distribution, finding that patterning can be

observed above a critical level of solute concentration. The time-scales of the fastest growing modes are consistent with experimental findings.

To investigate lymphangiogenesis in tumours, Friedman and Lolas [72] (see also [161]) propose a continuum model consisting of 8 reaction-diffusion equations for the evolution of the density of LECs and tumour cells, and the concentrations of ECM, VEGF-C, urokinase secreted by LECs and by tumour cells, and plasmin activated by LECs and tumour cells. The LECs and tumour cells migrate due to diffusion, chemotaxis and haptotaxis, and their proliferation is modelled by logistic growth. The LECs also proliferate due to VEGF-C-induced mitosis. The ECM diffuses, is degraded proteolytically by the plasmin, and re-establishes itself logistically. The authors study the model analytically to prove existence and uniqueness of the solution.

Finally, whilst they neglect any effects of lymphangiogenesis, we mention the recent article by Wu et al. [229] in which they investigate the effect of interstitial fluid pressure/flow (IFP/IFF) and the lymphatic network on vascularized tumour growth. Elevated IFP inside the tumour can block the delivery of nutrients or drugs, and may also affect the gradients of biochemical signals around the tumour. This work extends the model for angiogenesis and vascularized tumour growth in [119, 126, 127, 193, 231] already discussed in Section 4, to include IFF and drainage through the lymphatic system. The IFF is modelled using a two-phase continuum model, where the phases are fluid and cells, with a source term representing the release of IFF from the vasculature, and a sink term representing the drainage of IFF into the lymphatic network, which also allows for tumour stress-induced collapse of lymphatic vessels. The lymphatic network is modelled by a continuous density field, L, and is degraded by a proteolytic enzyme. In agreement with experimental observations, the IFP is elevated inside the tumour, leading to large IFF directed towards the surrounding tissue. Their results also indicated that the root cause of the plateau in the IFP inside the tumour is elevated interstitial hydraulic conductivity combined with poor lymphatic drainage.

Discussion

Independently from the applications, the classes of models presented in this review, continuous, mechanics-based models, cell-based models, and hybrid models provide complementary descriptions of vascular network formation. Indeed, while all the proposed mathematical approaches have shown a relevant degree of accuracy in reproducing selected phases of the vasculogenic process, it is evident that there are experimental evidences that can be explained only with a specific model, and not with the others. For instance, the continuous models described in Section 2 successfully described the early stages of vasculogenesis, dominated by the chemotactic and persistent motion of endothelial cells. However, it could not describe the mechanical interactions with the substratum (see Section 2.2), which is important to model the second phase, when cells adhere more strongly on the substratum. A similar difficulty would be encountered by cellular automata model and by cellular Potts models, though, starting from an energetic description of the elasticity of the substratum, some effects could be included. Plastic effects related to attachment and detachment mechanisms might be more difficult, though they have the advantage of focusing more closely

on achesion mechanics than continuous models. Individual cell-based models instead already include the interaction with the substratum, which however is usually rigid. Taking into account of its deformability should be possible.

Cell-based models in general allow a detailed description of the phenomenological behaviour of the single endothelial cells during the network formation and stabilization, of their morphological evolution and adhesion mechanics. Some dynamics, like vessel branching, anastomosis, pruning and vessel diameter remodelling are captured better by these types of models. Probably, some of them can also be described by cellular Potts models, but this has not been done yet.

An advantage of CPMs in their extended form is their ability to reproduce intracellular pathways, fundamental in determining the cell biophysical properties and behaviour. This is an essential feature, already included in some cellular automata, to link in a nested fashion the mesoscopic description of the behaviour of cells to their sub-cellular machineries. Subcellular protein cascades are activated or inactivated by chemical factors diffusing in the outer environment. The consequent hybrid characteristic is an essential ingredient of discrete, discretized or cell-based models, because chemical fields are more conveniently described by reaction-diffusion equations.

In conclusion, it is essential to perform a preliminary analysis of the mechanisms of vascular progression that need to be considered in order to have a realistic picture of the process of interest, before choosing the modelling technique most suitable to describe them.

Acknowledgements

This publication was based on work supported in part by Award No KUK-C1-013-04, made by King Abdullah University of Science and Technology (KAUST).

References

[1] Achen, M.G., Stacker, S.A., 2006. *Tumor lymphangiogenesis and metastatic spread - new players begin to emerge.* Int. J. Cancer, 119, 1755–1760.

[2] Adams, R.H., Alitalo, K., 2007. *Molecular regulation of angiogenesis and lymphangiogenesis.* Nat. Rev. Mol. Cell. Biol., 8, 464–478.

[3] Addison-Smith, B., McElwain, D.L.S., Maini, P.K., 2008. *A simple mechanistic model of sprout spacing in tumour-associated angiogenesis.* J. Theor. Biol., 250, 1–15.

[4] Alarcon, T., Byrne, H.M., Maini, P.K., 2003. *A cellular automaton model for tumour growth in an inhomegeneous environment.* J. Theor. Biol., 225, 257–274.

[5] Alarcon, T., Byrne, H.M., Maini, P.K., 2005. *A multiple scale model of tumour growth.* Multiscale Model. Sim., 3, 440–475.

[6] Alarcon, T., Byrne, H.M., Maini, P.K., 2005. *A design principle for vascular beds: the role of complex blood rheology.* Microvasc. Res., 69, 156–172.

[7] Alarcon, T., Owen, M.R., Byrne, H.M., Maini, P.K., 2006. *Multiscale modelling of tumour growth and therapy: the influence of vessels normalisation and chemotherapy.* Comp. Math. Methods Med., 7, 85–119.

[8] Alarcon, T., 2009. *Modelling tumour-induced angiogenesis: A review of individual-based models and multiscale approaches.* In **The Mathematics of Cancer and Developmental Biology**. M.A. Herrero, F. Giraldez, Eds. Contemporary Mathematics, 492, 45–47.

[9] Alitalo, K., 2011. *The lymphatic vasculature in disease.* Nature Med., 17, 1371-1380.

[10] Ambler, C.A., Nowicki, J.L., Burke, A.C., Bautch, V.L., 2001. *Assembly of trunk and limb blood vessels involves extensive migration and vasculogenesis of somite-derived angioblasts.* Dev. Biol., 234, 352–364.

[11] Ambrosi, D., Bussolino, F., Preziosi, L., 2005. *A review of vasculogenesis models.* J. Theor. Med., 6, 1–19.

[12] Ambrosi, D., Gamba, A., Serini, G., 2004. *Cell directional persistence and chemotaxis in vascular morphogenesis.* Bull. Math. Biol., 66, 1851–1873.

[13] Ambrosi, D., Preziosi, L., 2009. *Cell adhesion mechanisms and stress relaxation in the mechanics of tumours.* Biomech. Model. Mechanobiol., 8, 397–413.

[14] Anderson, A.R.A., Chaplain, M.A.J., 1998. *Continuous and discrete mathematical models of tumor-induced angiogenesis.* Bull. Math. Biol., 60, 857–900.

[15] Anderson, A.R.A., Chaplain, M.A.J., Rejniak, K.A., Eds. 2007. **Single-Cell-Based Models in Biology and Medicine**, Mathematics and Biosciences in Interaction (MBI) series, Birkhaüser-Verlag.

[16] Arnaoutova, I., Kleinman, H.K., 2010. *In vitro angiogenesis: Endothelial cell tube formation on gelled basement membrane extract.* Nat. Protoc., 5, 628–635.

[17] Astanin, S., Preziosi, L., 2009. *Mathematical modelling of the Warburg effect in tumour cords.* J. Theor. Biol., 258, 578–590.

[18] Astanin, S., Tosin, A., 2007. *Mathematical model of tumour cord growth along the source of nutrient.* Math. Model. Nat. Phenom., 2, 153–177.

[19] Aubert, M., Chaplain, M.A.J., McDougall, S.R., Devlin, A., Mitchell, C.A., 2011. *A continuum mathematical model of the developing murine retinal vasculature.* Bull. Math. Biol., 73, 2430–2451.

[20] Bahram, F., Claesson-Welsh, L., 2010. *VEGF-mediated signal transduction in lymphatic endothelial cells.* Pathophysiology, 17, 253–261.

[21] Balding, D., McElwain, D.L.S., 1985. *A mathematical model of tumor-induced capillary growth.* J. Theor. Biol., 114, 53–73.

[22] Baluk, P., Morikawa, S., Haskell, A., Mancuso, M., McDonald, D.M., 2003. *Abnormalities of basement membrane on blood vessels and endothelial sprouts in tumors.* Am. J. Pathol., 163, 1801–1815.

[23] Bartha, K., Rieger, H., 2006. *Vascular network remodeling via vessel cooption, regression and growth in tumors.* J. Theor. Biol., 241, 903–918.

[24] Bauer, A.L., Jackson, T.L., Jiang, Y., 2007. *A cell-based model exhibiting branching and anastomosis during tumor-induced angiogenesis.* Biophys. J., 92, 3105–3121.

[25] Bauer, A.L., Jackson, T.L., Jiang, Y., 2009. *Topography of extracellular matrix mediates vascular morphogenesis and migration speeds in angiogenesis.* PLOS Comp Biol., e1000445.

[26] Bayley, P., Ahlstrom, P., Martin, S.R., Forsen S., 1984. *The kinetics of calcium binding to calmodulin: Quin 2 and ANS stopped-flow fluorescence studies.* Biochem. Biophys. Res. Commun., 120, 185–191.

[27] Bearer, E.L., Lowengrub, J.S., Chuang, Y.L., Frieboes, H.B., Jin, F., Wise, S.M., Ferrari, M., Agus, D.B., Cristini, V., 2009. *Multiparameter computational modeling of tumor invasion.* Cancer Res., 69, 4493–4501.

[28] Berridge, M.J., Bootman, M.D., Roderick, H.L., 2003. *Calcium signalling: dynamics, homeostasis and remodelling.* Nature Rev. Mol. Cell Biol., 4, 517–529.

[29] Bertuzzi, A., Fasano, A., Gandolfi, A., 2005. *A mathematical model for tumor cords incorporating the flow of interstitial fluid.* Math. Models Methods Appl. Sci., 15, 1735–1777.

[30] Bertuzzi, A., Fasano, A., Gandolfi, A., Sinisgalli, C., 2007. *ATP production and necrosis formation in a tumour spheroid model.* Math. Model. Nat. Phenom., 2, 30–46.

[31] Bertuzzi, A., Fasano, A., Gandolfi, A., Sinisgalli, C., 2007. *Interstitial pressure and extracellular fluid motion in tumor cords.* Math. Biosci. Eng., 2, 445–460.

[32] Bertuzzi, A., Fasano, A., Gandolfi, A., Sinisgalli, C., 2008. *Reoxygenation and split-dose response to radiation in a tumour model with Krogh-type vascular geometry.* Bull. Math. Biol., 70, 992–1012.

[33] Betteridge, P., Owen, M.R., Alarcon, T., Maini, P.K., Byrne, H.M., 2006. *The impact of cell crowding and cell movement on vascular tumour growth.* Netw. Heter. Media., 1, 515–535.

[34] Boardman, K.C., Swartz, M.A., 2003. *Interstitial flow as a guide for lymphangiogenesis.* Circ. Res., 92, 801–808.

[35] Bruyère, F., Noël, A., 2010. *Lymphangiogenesis: in vitro and in vivo models.* FASEB J., 24, 8–21.

[36] Bussolati, B., Deregibus, M. C., Camussi, G., 2010. *Characterization of molecular and functional alterations of tumor endothelial cells to design anti-angiogenic strategies.* Curr. Vasc. Pharmacology, 8, 220–232.

[37] Bussolati, B., Deambrosis, I., Russo, S., Deregibus, M.C., Camussi, G., 2003. *Altered angiogenesis and survival in human tumor-derived endothelial cells.* FASEB J., 17, 1159–1161.

[38] Bussolati, B., Grange, C., Camussi, G., 2011. *Tumor exploits alternative strategies to achieve vascularization.* FASEB J., 25, 2874–2882.

[39] Bussolino, F., Arese, M., Audero, E., Giraudo, E., Marchio, S., Mitola, S., Primo, L., Serino, G., 2003. *Biological aspects in tumor angiogenesis.* In **Cancer Modeling and Simulation**, Preziosi, L., ed., Mathematical Biology and Medicine Sciences, Chapman and Hall/CRC, 1–16.

[40] Byrne, H.M., Chaplain M.A.J., 1995. *Mathematical models for tumour angiogenesis: Numerical simulations and nonlinear wave solutions.* Bull. Math. Biol., 57, 46–86.

[41] Byrne, H.M., Owen, M.R., Alarcon, T., Murphy, J., Maini, P.K., 2006. *Modelling the response of vascular tumours to anticancer therapies: a multiscale approach.* Math. Mod. Meth. App. Sci., 16, 1–25.

[42] Capasso, V., Morale, D., 2009. *Stochastic modelling of tumour-induced angiogenesis.* J. Math. Biol., 58, 219-233

[43] Carmeliet, P., Jain, R. K., 2000. *Angiogenesis in cancer and other diseases.* Nature, 407, 249–257.

[44] Carmeliet, P., 2005. *Angiogenesis in life, disease and medicine.* Nature, 438, 932–936.

[45] Caspi, O., Lesman, A., Basevitch, Y., Gepstein, A., Arbel, G., Habib, I.H., Gepstein, L., Levenberg, S., 2007. *Tissue engineering of vascularized cardiac muscle from human embryonic stem cells.* Circ. Res., 100, 263–272.

[46] Chaplain, M.A.J., McDougall, S.R., Anderson, A.R.A., 2006. *Mathematical modeling of tumor-induced angiogenesis.* Annu. Rev. Biomed. Eng., 8, 233-257.

[47] Chatelain, C., Balois, T., Ciarletta, P., Ben Amar, M., 2011. *Emergence of microstructural patterns in skin cancer: a phase separation analysis in a binary mixture.* New J. Phys., 13, 115013.

[48] Chen, T.T., Luque, A., Lee, S., Anderson, S. M., Segura, T., Iruela-Arispe, M.L., 2010. *Anchorage of VEGF to the extracellular matrix conveys differential signaling responses to endothelial cells.* J. Cell Biol., 188, 595–609.

[49] Chilibeck, P.D., Paterson, D.H., Cunningham, D.A., Taylor, A.W., Noble, E.G., 1997. *Muscle capillarization O2 diffusion distance, and VO2 kinetics in old and young individuals.* J. Appl. Physiol., 82, 63–69.

[50] Coniglio, A., de Candia, A., Di Talia, S., Gamba, A., 2004. *Percolation and Burgers' dynamics in a model of capillary formation.* Phys. Rev. E, 69, 051910.

[51] Cristini, V., Lowengrub, J.S., Nie, Q., 2003. *Nonlinear simulation of tumor growth.* J. Math. Biol., 46, 191–224.

[52] Cueni, L.N., Detmar, M., 2006. *New insights into the molecular control of the lymphatic vascular system and its role in disease.* J. Invest. Dermatol., 126, 2167–2177.

[53] De Angelis E., Preziosi, L., 2000. *Advection-diffusion models for solid tumour evolution in vivo and related free boundary problem.* Math. Models Meth. Appl. Sci., 10, 379–407.

[54] De Bock, K., Cauwenberghs, S., Carmeliet, P., 2011. *Vessel abnormalization: Another hallmark of cancer? Molecular mechanisms and therapeutic implications.* Curr. Opin. Genet. Dev., 21, 73 –79.

[55] Detmar, M., 2009. *Tumor and lymph node lymphangiogenesis.* In **From local invasion to metastatic cancer**, S.P.L. Leong ed., Current Clinical Oncology Vol. 6, Springer, 255–261.

[56] Dike, L.E., Chen, C.S., Mrksich, M., Tien, J., Whitesides, G.M., Ingber, D.E., 1999. *Geometric control of switching between growth, apoptosis, and differentiation during angiogenesis using micropatterned substrates. In Vitro.* Cell Dev. Biol. Anim., 35, 441–448.

[57] Drake, C. J., LaRue, A., Ferrara, N., Little, C. D., 2000. *VEGF regulates cell behavior during vasculogenesis.* Dev. Biol., 224, 178–188.

[58] Radszuweit, M., Block, M., Hengstler, J.G., Schöll, E., Drasdo, D., 2009. *Comparing the growth kinetics of cell populations in two and three dimensions.* Physical review. E, 79, 051907.

[59] Drasdo, D., Jagiella, N., Ramis-Conde, I., Vignon-Clementel, I., Weens, W., 2009. *Modeling steps from a benign tumor to an invasive cancer: examples of intrinsically multiscale problems.* In **From single scale-based models to multiscale modeling**, A. Chauviere, L. Preziosi, C. Verdier, Eds., CRC/Academic Press, 379–416.

[60] Ferrara, N., 2002. *VEGF and the quest for tumour angiogenesis factors.* Nat. Rev. Cancer, 2, 795–803.

[61] Ferrara, N., Gerber, H.P., LeCouter, J., 2003. *The biology of VEGF and its receptors.* Nature Med., 9, 669–676.

[62] Filbet, F., Laurençot, P., Perthame, B., 2004. *Derivation of hyperbolic models for chemosensitive movement.* J. Math. Biol., 50, 189–207.

[63] Fiorio Pla, A., Grange, C., Antoniotti, S., Tomatis, C., Merlino, A., Bussolati, B., Munaron, L., 2008. *Arachidonic acid-induced Ca2+ entry is involved in early steps of tumor angiogenesis.* Mol. Cancer Res., 6 (4), 535–545.

[64] Fiorio Pla, A., Munaron, L., 2001. *Calcium influx, arachidonic acid, and control of endothelial cell proliferation.* Cell Calcium, 30, 235–244.

[65] Fiorio Pla, A., Genova, T., Pupo, E., Tomatis, C., Genazzani, A., Zaninetti, R., Munaron, L., 2010. *Multiple roles of protein kinase a on arachidonic acidmediated Ca2+ entry and tumor-derived human endothelial cells migration.* Mol. Cancer Res., 8, 1466–1476.

[66] Fleury, M.E., Boardman, K.C., Swartz, M.A., 2006. *Autologous morphogen gradients by subtle interstitial flow and matrix interactions.* Biophys. J., 91, 113–121.

[67] Flory, J.P., 1953. **Principles of Polymer Chemistry**. Cornell University Press.

[68] Folkman, J., Haudenschild, C., 1980. *Angiogenesis in vitro.* Nature, 288, 551–556.

[69] Fong, G., Zhang, L., Bryce, D., Peng, J., 1999. *Increased hemangioblast commitment, not vascular disorganization, is the primary defect in flt-1 knock-out mice.* Development, 126, 3015–3025.

[70] Frieboes, H.B., Lowengrub, J.S., Wise, S.M., Zheng, X., Macklin, P., Bearer, E.L., Cristini, V., 2007. *Computer simulation of glioma growth and morphology.* NeuroImage, 37, S59–S70.

[71] Friedl, P., 2004. *Prespecification and plasticity: shifting mechanisms of cell migration.* Curr. Opin. Cell. Biol., 16, 14–23.

[72] Friedman, A., Lolas, G., *Analysis of a mathematical model of tumor lymphangiogenesis.* Math. Mod. Meth. Appl. Sci., 15 (2005) 95107.

[73] Fukumura, D., Duda, D. G., Munn, L. L., Jain, R. K., 2010. *Tumor microvasculature and microenvironment: Novel insights through intravital imaging in pre-clinical models.* Microcirculation, 17, 206–225.

[74] Gamba, A., Ambrosi, D., Coniglio, A., de Candia, A., di Talia, S., Giraudo, E., Serini, G., Preziosi, L., Bussolino, F., 2003. *Percolation, morphogenesis, and Burgers dynamics in blood vessel formation.* Phys. Rev. Lett., 90, 101–118.

[75] Gevertz, J.L., Torquato, S., 2006. *Modeling the effects of vasculature evolution on early brain tumor growth.* J. Theor. Biol., 243, 517–531.

[76] Glazier, J.A., Balter, A., Merks, R.M.H., Poplawski, N.J., Swat, M., 2007. *The Glazier-Graner-Hogeweg model: extension, future direction, and opportunitites for further study.* Single-Cell-Based Model Biol. Med., 4, 157–167 (Chapter II).

[77] Glazier, J.A., Balter, A., Poplawski, N.J., 2007. *Magnetization to morphogenesis: a brief history of the Glazier-graner-Hogeweg model.* In **Single-Cell-Based Models in Biology and Medicine**, A.R.A. Anderson, M.A.J. Chaplain, K.A. Rejniak eds., Mathematics and Biosciences in Interactions, Birkhaüser, 79–106.

[78] Glazier, J. A., Graner, F., 1993. *Simulation of the differential adhesion driven rearrangement of biological cells.* Phys. Rev. E, 47, 2128–2154.

[79] Goel, S., Duda, D.G., Xu, L., Munn, L.L., Boucher, Y., Fukumura, D., Jain, R.K., 2011. *Normalization of the vasculature for treatment of cancer and other diseases.* Physiol. Rev., 91, 1071–1121.

[80] Goto, Y., Miura, M., Iijima, T., 1996. *Extrusion mechanisms of intracellular Ca2+ in human aortic endothelial cells.* Eur. J. Pharmacol., 314, 185–192.

[81] Graner, F., Glazier, J.A., 1992. *Simulation of biological cell sorting using a two dimensional extended Potts model.* Phys. Rev. Lett., 69, 2013–2017.

[82] Grange, C., Bussolati, B., Bruno, S., Fonsato, V., Sapino, A., Camussi, G., 2006. *Isolation and characterization of human breast tumor-derived endothelial cells.* Oncol. Rep., 15, 381–386.

[83] Grant, D., Tashiro, K., Segui-Real, B., Yamada, Y., Martin, G., Kleinman, H., 1989. *Two different laminin domains mediate the differentiation of human endothelial cells into capillary-like structures in vitro.* Cell, 58, 933–943.

[84] Griffith, L.G., Naughton, G., 2002. *Tissue engineering: Current challenges and expanding opportunities.* Science, 295, 1009–1014.

[85] Guangqi, E., Cao, Y., Bhattacharya, S., Dutta, S., Wang, E., Mukhopadhyay, D., 2012. *Endogenous vascular endothelial growth factor-A (VEGF-A) maintains endothelial cell homeostasis by regulating VEGF receptor-2 transcription.* J. Biol. Chem., 287, 3029-3041.

[86] Guyton, A., Hall, J. 2000. **Textbook of Medical Physiology.** W.B. Saunders, St. Louis.

[87] Helm, C.L., Fleury, M.E., Zisch, A.H., Boschetti, F., Swartz, M.A., 2005. *Synergy between interstitial flow and VEGF directs capillary morphogenesis in vitro through a gradient amplification mechanism.* Proc. Natl. Acad. Sci. U.S.A., 102, 15779–15784.

[88] Helm, C.L., Zisch, A., Swartz, M.A., 2007. *Engineered blood and lymphatic capillaries in 3-D VEGF-fibrin-collagen matrices with interstitial flow.* Biotechnol. Bioeng., 96, 167–176.

[89] Helmlinger, G., Endo, M., Ferrara, N., Hlatky, L., Jain, R., 2000. *Formation of endothelial cell networks.* Nature, 405, 139–141.

[90] Hillen, T., Painter, K.J., 2009. *A user's guide to PDE models for chemotaxis.* J. Math. Biol., 58, 183–217.

[91] Hogea, C.S., Murray, B.T., Sethian, J.A., 2006. *Simulating complex tumor dynamics from avascular to vascular growth using a general level-set method.* J. Math. Biol., 53, 86–134.

[92] Holmes, M., Sleeman, B., 2000. *A mathematical model of tumor angiogenesis incorporating cellular traction and viscoelastic effects.* J. Theor. Biol., 202, 95–112.

[93] Hryshko, L.V., Philipson, K.D., 1997. *Sodium-calcium exchange: recent advances.* Basic Res. Cardiol., 92, 45–51.

[94] Huang, S., Brangwynne, C. P., Parker, K. K., Ingber, D. E., 2005. *Symmetry-breaking in mammalian cell cohort migration during tissue pattern formation: role of random-walk persistence.* Cell Motil. Cytoskeleton, 61, 201–213.

[95] Hudon, V., Berthod, F., Black, A.F., Damour, O., Germain, L., Auger, F.A., 2003. *A tissue-engineered endothelialized dermis to study the modulation of angiogenic and angiostatic molecules on capillary-like tube formation in vitro.* Br. J. Dermatol., 148, 1094–1104.

[96] Jain H.V., Nor J.E., Jackson, T.L., 2008. *Modeling the vegf-bcl-2-cxcl8 pathway in intratumoral angiogenesis.* Bull. Math. Biol., 70, 89–117.

[97] Jain, R.K., 2001. *Normalizing tumor vasculature with anti-angiogenic therapy: A new paradigm for combination therapy.* Nature Med., 7, 987–989.

[98] Jain, R.K., 2005. *Normalization of tumor vasculature: an emerging concept in antiangiogenic therapy.* Science, 307, 58–62.

[99] Jain, R.K., Au, P., Tam , J., Duda, D.G., Fukumura, D., 2005. *Engineering vascularized tissue.* Nat. Biotechnol., 23, 821-823.

[100] Ji, R.-C., 2006. *Lymphatic endothelial cells, lymphangiogenesis, and extracellular matrix.* Lymphat. Res. Biol., 4, 83–100.

[101] Karpanen, T., Alitalo, K., 2008. *Molecular biology and pathology of lymphangiogenesis.* Annu. Rev. Pathol., 3, 367–397.

[102] Karpanen, T., Alitalo, K., 2001. *Lymphatic vessels as targets of tumor therapy?* J. Exp. Med., 194, F37–42.

[103] Kimura, H., Esumi, H., 2003. *Reciprocal regulation between nitric oxide and vascular endothelial growth factor in angiogenesis.* Acta Biochim. Pol., 50, 49–59.

[104] Klingauf, J., Neher, E., 1997. *Modeling buffered Ca^{2+} diffusion near the membrane: implications for secretion in neuroendocrine cells.* Biophys. J., 72, 674–690.

[105] Köhn-Luque, A., de Back, W., Starruss, J., Mattiotti, A., Deutsch, A., Prez-Pomares, J. M., Herrero, M. A., 2011. *Early embryonic vascular patterning by matrix-mediated paracrine signalling: a mathematical model study.* PLoS One, 6, e24175.

[106] Kowalczyk, R., 2005. *Preventing blow-up in a chemotaxis model.* J. Math. Anal. Appl., 305, 566–588.

[107] Krogh, A., 1919. *The number and distribution of capillaries in muscle with calculations of the oxygen pressure head necessary for supplying the tissue.* J. Physiol., 52, 409–415.

[108] Kubota, Y., Kleinman, H., Martin, G., Lawley, T., 1988. *Role of laminin and basement membrane in the morphological differentiation of human endothelial cells into capillary-like structures.* J. Cell Biol., 107, 1589–1598.

[109] Lanza, V., Ambrosi, D., Preziosi, L., 2006. *Exogenous control of vascular network formation in vitro: A mathematical model.* Netw. Heter. Media, 1, 621–637.

[110] Levenberg, S., Rouwkema, J., Macdonald, M., Garfein, E.S., Kohane, D.S., Darland, D.C., Marini, R., van Blitterswijk, C.A., Mulligan, R.C., D'Amore P.A., Langer, R., 2005. *Engineering vascularized skeletal muscle tissue.* Nature Biotechnol., 23, 879–884.

[111] Levine, H., Sleeman, B., 1997. *A system of reaction diffusion equations arising in the theory of reinforced random walks.* SIAM J. Appl. Math., 57, 683–730.

[112] Levine, H.A., Pamuk, S., Sleeman B.D., Nilsen-Hamilton, M., 2001. *Mathematical modeling of capillary formation and development in tumor angiogenesis: penetration into the stroma.* Bull. Math. Biol., 63, 801–863.

[113] Levine, H., Sleeman, B., Nilsen-Hamilton, M., 2001. *Mathematical modeling of the onset of capillary formation initiating angiogenesis.* J. Math. Biol., 42, 195–238.

[114] Levine, H.A., Smiley, M.W., Tucker, A.L., Nilsen-Hamilton, M.A., 2006. *Mathematical model for the onset of avascular tumor growth in response to the loss of p53 function.* Cancer Informatics, 2, 163–188.

[115] Levine, H.A., Tucker, A.L., Nilsen-Hamilton, M.A., 2002. *Mathematical model for the role of cell signal transduction in the initiation and inhibition of angiogenesis.* Growth Factors, 20, 155-175.

[116] Lloyd, B.A., Szczerba, D., Szkely, G., 2007. *A coupled finite element model of tumor growth and vascularization.* MICCAI, 2, 874–881.

[117] Lowengrub, J.S., Frieboes, H.B., Jin, F., Chuang, Y.L., Li, X., Macklin, P., Cristini, V., 2010. *Nonlinear modelling of cancer: bridging the gap between cells and tumours.* Nonlinearity, 23, R1–R9.

[118] Machado, M.J.C., Watson, M.G., Devlin, A.H., Chaplain, M.A.J., McDougall, S.R., Mitchell, C.A., 2011. *Dynamics of angiogenesis during wound healing: a coupled in vivo and in silico study.* Microcirculation, 18, 183–197.

[119] Macklin, P., McDougall, S., Anderson, A.R.A., Chaplain, M.A.J., Cristini, V., Lowengrub, J., 2009. *Multiscale modeling and nonlinear simulation of vascular tumour growth.* J. Math. Biol., 58, 765–798.

[120] Mandriota, S.J., Jussila, L., Jeltsch, M., Compagni, A., Baetens, D., Prevo, R., Banerji, S., Huarte, J., Montesano, R., Jackson, D.G., Orci, L., Alitalo, K., Christofori, G., Pepper, M.S., *Vascular endothelial growth factor-C-mediated lymphangiogenesis promotes tumour metastasis.* EMBO J., 20, 672–682.

[121] Manoussaki, D., 2004. *A mechanochemical model of vasculogenesis and angiogenesis.* Math. Model. Num. Anal., 37, 581–599.

[122] Manoussaki, D., Lubkin, S. R., Vernon, R. B., Murray, J. D., 1996. *A mechanical model for the formation of vascular networks in vitro.* Acta Biotheoretica, 44, 271–282.

[123] Mantzaris, N.V., Webb, S., Othmer, H.G., 2004. *Mathematical modeling of tumor-induced angiogenesis.* J. Math. Biol., 49, 111–187.

[124] Marée, A. F. M., Grieneisen, V. A., Hogeweg, P., 2007. *The Cellular Potts Model and biophysical properties of cells, tissues and morphogenesis.* In **Single-Cell-Based Models in Biology and Medicine**, A.R.A. Anderson, M.A.J. Chaplain, K.A. Rejniak, eds., Mathematics and Biosciences in Interactions, Birkhaüser, 107–136.

[125] Markus, M., Bohm, D., Schmick, M., 1999. *Simulation of vessel morphogenesis using cellular automata.* Math. Biosci., 156, 191-206.

[126] McDougall, S.R., Anderson, A.R.A., Chaplain, M.A.J., 2006. *Mathematical modeling of dynamic adaptive tumour-induced angiogenesis: Clinical applications and therapeutic targeting strategies.* J. Theor. Biol., 241, 564–589.

[127] McDougall, S.R., Anderson, A.R.A., Chaplain, M.A.J., Sherratt, J., 2002. *Mathematical modelling of flow through vascular networks: implications for tumour-induced angiogenesis and chemotherapy strategies.* Bull. Math. Biol., 64, 673–702.

[128] McDougall, S.R., Chaplain, M.A.J., Stephanou, A., Anderson, A.R.A., 2010. *Modelling the impact of pericyte migration and coverage of vessels on the efficacy of vascular disrupting agents.* Math. Model. Nat. Phenom., 5, 163–202.

[129] Merks, R.M.H., Brodsky, S.V., Goligorksy, M.S., Newman, S.A., Glazier, J.A., 2006. *Cell elongation is key to in silico replication of in vitro vasculogenesis and subsequent remodeling.* Dev. Biol., 289, 44–54.

[130] Merks, R. M. H., Glazier, J. A., 2006. *Dynamic mechanisms of blood vessel growth.* Inst. Phys. Publ., 19, C1–C10.

[131] Merks, R.M.H., Glazier, J.A., Brodsky, S.V., Goligorksy, M.S., Newman, S.A., 2006. *Cell elongation is key to in silico replication of in vitro vasculogenesis and subsequent remodeling.* Develop. Biol., 289, 44–54.

[132] Merks, R.M.H., Perryn, E.D., Shirinifard, A., Glazier, J.A., 2008. *Contact-inhibited chemotactic motility: role in de novo and sprouting blood vessel growth.* PLOS Comp. Biol., 4, e1000163.

[133] Merks, R.M.H., Newman, S.A., Glazier, J.A., 2004. *Cell-oriented modeling of in vitro capillary development.* Lect. Notes Comput. Sc., 3305, 425–434.

[134] Milde, F., Bergdorf, M., Koumoutsakos. P., 2008. *A hybrid model for three-dimensional simulations of sprouting angiogenesis.* Biophys. J., 95, 3146–3160.

[135] Moon, J.J., West, J.L., 2008. *Vascularization of engineered tissues: approaches to promote angiogenesis in biomaterials.* Curr. Top. Med. Chem., 8, 300–310.

[136] Mottola, A., Antoniotti, S., Lovisolo, D., Munaron, L., 2005. *Regulation of noncapacitative calcium entry by arachidonic acid and nitric oxide in endothelial cells.* FASEB J., 19, 2075–2077.

[137] Muller, Y., Christinger, H., Keyt, B. and de Vos, A., 1997. *The crystal structure of vascular endothelial growth factor (VEGF) refined to 1.93 Åresolution: multiple copy flexibility and receptor binding.* Structure, 5, 1325.

[138] Munaron, L., 2002. *Calcium signalling and control of cell proliferation by tyrosine kinase receptors (review).* Int. J. Mol. Med., 10, 671–676.

[139] Munaron, L., 2006. *Intracellular calcium, endothelial cells and angiogenesis.* Recent Patents Anticancer Drug Discov., 1, 105–119.

[140] Munaron, L., Antoniotti, S., Distasi, C., Lovisolo, D., 1997. *Arachidonic acid mediates calcium influx induced by basic fibroblast growth factor in Balb-c 3T3 fibroblasts.* Cell Calcium, 22, 179–188.

[141] Munaron, L., Fiorio Pla, A., 2000. *Calcium influx induced by activation of tyrosine kinase receptors in cultured bovine aortic endothelial cells.* J. Cell Physiol., 185, 454–463.

[142] Munaron, L., 2009. *A tridimensional model of proangiogenic calcium signals in endothelial cells.* The Open Biology J., 2, 114–129.

[143] Munaron, L., Fiorio Pla, A., 2000. *Endothelial calcium machinery and angiogenesis: understanding physiology to interfere with pathology.* Current Medicinal Chemistry, 16, 4691–4703.

[144] Murray, J.D., Oster, G.F., 1984. *Cell traction models for generation of pattern and form in morphogenesis.* J. Math. Biol., 19, 265–279.

[145] Murray, J.D., Oster, G.F., 1984. *Generation of biological pattern and form.* J. Math. Appl. Med. Biol., 1, 51–75.

[146] Murray, J.D., Oster, G.F., Harris, A.K., 1983. *A mechanical model for mesenchymal morphogenesis.* J. Math. Biol., 17, 125–129.

[147] Murray, J.D., Manoussaki, D., Lubkin, S.R., Vernon, R.B., 1998. *A mechanical theory of in vitro vascular network formation.* In **Vascular Morphogenesis: In Vivo, In Vitro and In Mente**, C. Little, V. Mironov and H. Sage, Eds., Birkhäuser, Boston.

[148] Murray, J.D., Swanson, K.R., 1999. *On the mechanochemical theory of biological pattern formation with applications to wound healing and angiogenesis.* In **On Growth and Form: Spatio-temporal Pattern Formation in Biology**, M.A.J. Chaplain, G.D. Singh, J.C. McLachlan, Eds., J. Wiley and Sons.

[149] Murray, J.D., 2003. *On the mechanical theory of biological pattern formation with application to vasculogenesis.* Comp. Rrnd. Biologies, 326, 2239–2252.

[150] Namy, P., Ohayon, J., Traqui, P., 2004. *Critical conditions for pattern formation and in vitro tubulogenesis driven by cellular traction fields.* J. Theor. Biol., 227, 103–120.

[151] Neufeld, G., Cohen, T., Gengrinovitch, S., Poltorak, Z., 1999. *Vascular endothelial growth factor (VEGF) and its receptors.* Faseb J., 13, 9–22.

[152] Ng, C.P., Helm, C.-L.E., Swartz, M.A., 2004. *Interstitial flow differentially stimulates blood and endothelial cell morhpogenesis in vitro.* Microvas. Res., 68, 258–264.

[153] Norrmén, C., Tammela, T., Petrova, T.V., Alitalo, K., 2011. *Biological basis of therapeutic lymphangiogenesis.* Circulation, 123, 1335-1351.

[154] Orme, M.E., Chaplain, M.A.J., 1997. *Two-dimensional models of tumour angiogenesis and anti-angiogenesis strategies.* Math. Med. Biol., 14, 189–205.

[155] Oster, G. F., Murray, J. D., Harris, A. K., 1983. *Mechanical aspects of mesenchymal morphogenesis. Cell traction models for generation of pattern and form in morphogenesis.* J. Embryol. Exp. Morph., 78, 83–125.

[156] Othmer, H., Stevens, A., 1997. *Aggregation, blowup and collapse: The ABC's of generalized taxis.* SIAM J. Applied Math., 57, 1044–1081.

[157] Owen, M.R., Alarcon, T., Maini, P.K., Byrne, H.M., 2009. *Angiogenesis and vascular remodelling in normal and cancerous tissues.* J. Math. Biol., 58, 689–721.

[158] Parker, B.S., Argani, P., Cook, B.P., Liangfeng, H., Chartrand, S.D., Zhang, M., Saha, S., Bardelli, A., Jiang, Y., St Martin, T.B., Nacht, M., Teicher, B.A., Klinger, K.W., Sukumar, S., Madden, S.L., 2004. *Alterations in vascular gene expression in invasive breast carcinoma.* Cancer Res., 64, 7857–7866.

[159] Parsa, H., Upadhyay, R., Sia, S.K., 2011. *Uncovering the behaviors of individual cells within a multicellular microvascular community.* Proc. Natl. Acad. Sci. U.S.A., 108, 5133–5138.

[160] Pepper, M.S., 2001. *Lymphangiogenesis and tumor metastasis: myth or reality?* Clin. Cancer Res., 7, 462–468.

[161] Pepper, M.S., Lolas, G., 2008. *The lymphatic vascular system in lymphangiogenesis, invasion and metastasis: a mathematical approach.* In **Selected topics in cancer modeling: Genesis, Evolution, Immune Competition, and Therapy**, E. De Angelis, M.A.J. Chaplain, N. Bellomo, Eds., Birkhäuser, 255–276.

[162] Perfahl, H., Byrne, H.M., Chen, T., Estrella, V., Alarcon, T., Lapin, A., Gatenby, R.A., Gillies, R.J., Lloyd, M.C., Maini, P.K. Reuss, M., Owen, M.R., 2011. *Multiscale modelling of vascular tumour growth in 3D: The roles of domain size and boundary conditions.* PLoS One, 6, e14790.

[163] Peterson, J.W., Carey, G.F., Knezevic, D.J., Murray, B.T., 2007. *Adaptive finite element methodology for tumour angiogenesis modelling.* Intl. J. Numer. Methods Eng., 69, 1212–1238.

[164] Plank M.J., Sleeman, B.D., 2003. *A reinforced random walk model of tumour angiogenesis and anti-angiogenic strategies.* Math. Med. Biol., 20, 135–181.

[165] Plank M.J., Sleeman, B.D., 2004. *Lattice and non-lattice models of tumour angiogenesis.* Bull. Math. Biol., 66, 1785–1819.

[166] Plank M.J., Sleeman, B.D., 2004. *A mathematical model of tumour angiogenesis, regulated by vascular endothelial growth factor and the angiopoietins.* J. Theor. Biol., 229, 435–454.

[167] Pluen, A., Netti, P.A., Jain, R.K., Berk, D.A., 1999. *Diffusion of macromolecules in agarose gels: comparison of linear and globular configurations.* Biophys. J., 77, 542–552.

[168] Preziosi, L., Ambrosi, D., Verdier, C., 2010. *An elasto-visco-plastic model of cell aggregates.* J. Theor. Biol., 262, 35–47.

[169] Pries, A.R., Secomb, T.W., Gaehtgens, P., 1996. *Biophysical aspects of blood flow in the microvasculature.* Cardiovasc. Res., 32, 654–667.

[170] Pries, A.R., Reglin, B., Secomb, T.W., 2001. *Structural adaptation of microvascular networks: functional roles of adaptive responses.* Am. J. Physiol. Heart Circ. Physiol., 281, H1015–H1025.

[171] Pries, A.R., Reglin, B., Secomb, T.W., 2001. *Structural adaptation of vascular networks role of the pressure response.* Hypertension, 38, 1476–1479.

[172] Pries, A.R., Secomb, T.W., Gaehtgens, P., 1998. *Structural adaptation and stability of microvascular networks: Theory and simulations.* Am. J. Physiol., 275, H349–H360.

[173] Pries, A.R., Secomb, T.W., 2005. *Control of blood vessel structure: insights from theoretical models.* Am. J. Physiol. Heart Circ. Physiol., 288, 1010–1015.

[174] Pries, A.R., Secomb, T.W., 2008. *Modeling structural adaptation of microcirculation.* Microcirculation, 15, 753–764.

[175] Risau, W., Flamme, I., 1995. *Vasculogenesis.* Annu. Rev. Cell Dev. Biol., 11, 73–91.

[176] Roose, T., Fowler, A.C., 2008. *Network Development in Biological Gels: Role in Lymphatic Vessel Development.* Bull. Math. Biol., 70, 1772-1789.

[177] Ruhrberg, C., Gerhardt, H., Golding, M., Watson, R., Ioannidou, S., Fujisawa, H., Betsholtz, C., Shima, D., 2002. *Spatially restricted patterning cues provided by heparin-binding VEGF-A control blood vessel branching morphogenesis.* Gen. Devel., 16, 2684–2698.

[178] Saharinen, P., Tammela, T., Karkkainen, M.J., Alitalo, K., 2004. *Lymphatic vasculature: development, molecular regulation and role in tumor metastasis and inflammation* Trends Immunol., 25, 387–395.

[179] Sambeth, R., Bamgaertner, A., 2001. *Autocatalytic polymerization generates persistent random walk of crawling cells.* Phys. Rev. Lett., 86, 5196–5199.

[180] Sansone, B.C., Scalerandi, M., Condat, C.A., 2001. *Emergence of taxis and synergy in angiogenesis.* Phys. Rev. Lett., 87, 128102.

[181] Savill, N. J., Hogeweg, P., 1997. *Modelling morphogenesis: from single cells to crawling slugs.* J. Theor. Biol., 184, 118–124.

[182] Schmidt, A., Brixius, K., Bloch, W., 2007. *Endothelial precursor cell migration during vasculogenesis.* Circ. Res., 101, 125–136.

[183] Scianna, M., Merks, R. M. H., Preziosi, L., Medico, E., 2009. *Individual cell-based models of cell scatter of ARO and MLP-29 cells in response to hepatocyte growth factor.* J. Theor. Biol., 260, 151–160.

[184] Scianna, M., Munaron, L., Preziosi, L., 2011. *A multiscale hybrid approach for vasculogenesis and related potential blocking therapies.* Prog. Biophys. Mol. Biol., 106, 450–462.

[185] Scianna, M., Munaron, L., 2011. *Multiscale model of tumor-derived capillary-like network formation.* Netw. Heterog. Media, 6, 597–624.

[186] Seaman, S., Stevens, J., Yang, M. Y., Logsdon, D., Graff-Cherry, C., St Croix, B., 2007. *Genes that distinguish physiological and pathological angiogenesis.* Cancer Cell, 11, 539–554.

[187] Serini, G., Ambrosi, D., Giraudo, E., Gamba, A., Preziosi, L., Bussolino, F., 2003. *Modeling the early stages of vascular network assembly.* EMBO J., 22, 1771–1779.

[188] Sleeman, B.D., Wallis, I.P., 2002. *Tumour induced angiogenesis as a reinforced random walk: Modelling capillary network formation without endothelial cell proliferation.* Math. Comp. Model., 36, 339–358.

[189] Stacker, S.A., Achen, M.G., Jussila, L., Baldwin, M.E., Alitalo, K., 2002. *Lymphangiogenesis and cancer metastasis.* Nat. Rev. Cancer, 2, 573–583.

[190] Stamper, I.J,, Byrne, H.M., Owen, M.R., Maini, P.K., 2007. *Modelling the role of angiogenesis and vasculogenesis in solid tumour growth.* Bull. Math. Biol., 69, 27372772.

[191] Steinberg, M. S., 1963. *Reconstruction of tissues by dissociated cells. Some morphogenetic tissue movements and the sorting out of embryonic cells may have a common explanation.* Science, 141, 401–408.

[192] Steinberg, M. S., 1970. *Does differential adhesion govern self-assembly processes in histogenesis? Equilibrium configurations and the emergence of a hierarchy among populations of embryonic cells.* J. Exp. Zool., 173, 395–433.

[193] Stephanou, A., McDougall, S.R., Anderson, A.R.A., Chaplain, M.A.J., 2005. *Mathematical modelling of flow in 2d and 3d vascular networks: applications to anti-angiogenic and chemotherapeutic drug strategies.* Math. Comput. Model., 41, 1137–56.

[194] Stephanou, A., McDougall, S.R., Anderson, A.R.A., Chaplain, M.A.J., 2006. *Mathematical modeling of the influence of blood rheological properties upon adaptive tumour-induced angiogenesis.* Math. Comput. Model., 44, 96–123.

[195] Straume, O., Salvesen, H. B., Akslen, L. A., 1999. *Angiogenesis is prognostically important in vertical growth phase melanomas.* Int. J. Oncol., 15, 595–599.

[196] Stroock, A.D., Fischbach, C., 2010. *Microfluidic culture models of tumor angiogenesis.* Tissue Eng. A., 16, 2143–2146.

[197] Sun, S., Wheeler, M.F., Obeyesekere, M., Patrick, C. Jr., 2005. *Multiscale angiogenesis modeling using mixed finite element methods*. Multiscale Model. Simul., 4, 1137–1167.

[198] Sun, S., Wheeler, M.F., Obeyesekere, M., Patrick, C. Jr., 2005. *A deterministic model of growth factor-induced angiogenesis*. Bull. Math. Biol., 67, 313–337.

[199] Swartz, M.A., 2001. *The physiology of the lymphatic system*. Adv. Drug Deliver. Rev., 50, 3–20.

[200] Swartz, M.A., Skobe, M., 2001. *Lymphatic function, lymphangiogenesis, and cancer metastasis*. Microsc. Res. Techniq., 55, 92–99.

[201] Szabo, A., Perryn, E.D., Czirok, A. 2007. *Network formation of tissue cells via preferential attraction to elongated structures*. Phys. Rev. Lett., 98, 038102.

[202] Szabo, A., Mehes, E., Kosa, E., Czirok, A., 2008. *Multicellular sprouting in vitro*, Biophys. J., 95, 2702–2710.

[203] Szczerba, D., Szkely, G., 2005. *Simulating vascular systems in arbitrary anatomies*. MICCAI, 641–648.

[204] Szczerba, D., Szkely, G., 2002. *Macroscopic modeling of vascular systems*. MICCAI, 284–292.

[205] Tammela, T., Alitalo, K., 2010. *Lymphangiogenesis: Molecular mechanisms and future promise*. Cell, 140, 460–476.

[206] Tomatis, C., Fiorio Pla, A., Munaron, L., 2007. *Cytosolic calcium microdomains by arachidonic acid and nitric oxide in endothelial cells.* Cell Calcium, 41 (3), 261–269.

[207] Tong, S., Yuan, F., 2001. *Numerical simulations of angiogenesis in the cornea*. Microvasc. Res., 61, 14–27.

[208] Tosin, A., Ambrosi, D., Preziosi, L., 2006. *Mechanics and chemotaxis in the morphogenesis of vascular networks.* Bull. Math. Biol., 68, 1819–1836.

[209] Tranqui, L., Traqui, P., 2000. *Mechanical signalling and angiogenesis. The integration of cell-extracellular matrix couplings.* C.R. Acad. Sci. Paris, Science de la Vie, 323, 31–47.

[210] Travasso, R.D.M., Corvera Poire, E., Castro, M., Rodriguez-Manzaneque, J.C., Hernandez-Machado, A., 2011. *Tumor Angiogenesis and Vascular Patterning: A Mathematical Model*. PLOS One, 6, e19989.

[211] Tremblay, P.L., Hudon, V., Berthod, F., Germain, L., Auger, F.A., 2005. *Inosculation of tissue-engineered capillaries with the host's vasculature in a reconstructed skin transplanted on mice*. Am. J. Transplant, 5, 1002–1010.

[212] Vailhé, B., Vittet, D., Feige, J. J., 2001. *In vitro models of vasculogenesis and angiogenesis*. Lab. Investig., 81, 439–452.

[213] Valant, P. A., Adjei, P. N., Haynes, D. H., 1992. *Rapid Ca2+ extrusion via the Na+/Ca2+ exchanger of the human platelet.* J. Membr. Biol., 130, 63–82.

[214] Verbridge, S.S., Choi, N.W., Zheng, Y., Brooks, D.J., Stroock, A.D., Fischbach, C., 2010. *Oxygen-controlled three-dimensional cultures to analyze tumor angiogenesis*. Tissue Eng. A, 16, 2133–2141.

[215] Vernon, R., Angello, J., Iruela-Arispe, M.-L., Lane, T., Sage, E.-H., 1992. *Reorganization of basement membrane matrices by cellular traction promotes the formation of cellular networks in vitro.* Lab. Invest., 66, 536–546.

[216] Vernon, R., Lara S. L., Drake C. J., Iruela-Arispe M.-L., Angello J., Little C. D. and Sage E.-H., 1995. *Organized type 1 collagen influences of endothelial patterns during spontaneous angiogenesis in vitro: planar cultures as models of vascular development.* In Vitro Vascular and Developmental Biology, 31, 120–131.

[217] Vernon, R., Sage, E.-H., 1995. *Between molecules and morphology. extracellular matrix and creation of vascular form.* Amer. J. Path., 1447, 873–883.

[218] Walter, M., Cook, W., Ealick, S., Nagabhushan, T., Trotta, P. and Bugg, C., 1992. *Three-dimensional structure of recombinant human granulocyte-macrophage colony-stimulating factor*, J. Mol. Biol., 224, 1075–1085.

[219] Watson, E. L., Jacobson, K. L., Singh, J. C., Di Julio, D. H., 2004. *Arachidonic acid regulates two Ca2+ entry pathways via nitric oxide.* Cell Signal., 16, 157–165.

[220] Watson, M.G., McDougall, S.R., Chaplain, M.A.J., Devlin, A.H., Mitchell, C.A., 2012. *Dynamics of angiogenesis during murine retinal development: a coupled in vivo and in silico study.* J.R. Soc. Interface. doi: 10.1098/rsif.2012.0067.

[221] Webb, D.J., Horwitz, A.F., 2003. *New dimensions in cell migration.* Nature Cell Biol., 5, 690–692.

[222] Welter, M., Bartha, K., Rieger, H., 2008. *Emergent vascular network inhomogenities and resulting blood flow patterns in a growing tumor.* J. Theor. Biol., 250, 257–280.

[223] Welter, M., Bartha, K., Rieger, H., 2009. *Vascular remodelling of an arterio-venous blood vessel network during solid tumor growth.* J. Theor. Biol., 259, 405–422.

[224] Welter, M., Bartha, K., Rieger, H., 2010. *Physical determinants of vascular network remodeling during tumor growth.* Europ. Phys. J. E, 33, 149–163.

[225] Whitaker, N., Harrington, H.A.,Maier, M., Naidoo, L., Kevrekidis, P.G., 2007. *A hybrid model for tumor-induced angiogenesis in the cornea in the presence of inhibitors.* Math. Comput. Modelling, 46, 513–524.

[226] Wiig, H., Keskin, D., Kalluri, R., 2010. *Interaction between the extracellular matrix and lymphatics: Consequences for lymphangiogenesis and lymphatic function.* Matrix Biol., 29, 645–656.

[227] Wise, S.M., Lowengrub, J.S., Frieboes, H.B., Cristini, V., 2008. *Three-dimensional multispecies nonlinear tumor growth: I. Model and numerical method.* J. Theor. Biol., 253, 524–543.

[228] Wolf, K., Mazo, I., Leung, H., Engelke, K., von Andrian, U. H., Deryugina, E. I., Strongin, A. Y., Bröcker, E.-B., Friedl, P., 2003. *Compensation mechanism in tumor cell migration: mesenchymal–ameboid transition after blocking of pericellular proteolysis.* J. Cell. Biol., 160, 267–277.

[229] Wu, M., Frieboes, H.B., McDougall S.R., Chaplain, M.A.J., Cristini, V., Lowengrub, J. The effect of interstitial pressure on tumor growth: coupling with the blood and lymphatic vascular systems. Submitted.

[230] Zhao, G., Wu, J., Xu, S., Collins, M.W., Long, Q., Koenig, C.S., Jiang, Y., Wang, J., Padhani, A.R., 2007. *Numerical simulation of blood flow and interstitial fluid pressure in solid tumor microcirculation based on tumor induced angiogenesis.* Mech. Sin., 23, 477–483.

[231] Zheng, X.,Wise, S.M., Cristini, V., 2005. *Nonlinear simulation of tumor necrosis, neo-vascularization and tissue invasion via an adaptive finite-element/level-set method.* Bull. Math. Biol., 67, 211–259.

[232] Zheng, Y., Chen, J., Craven, M., Choi, N.W., Totorica, S., Diaz-Santana, A., Kermani, P., Hempstead, B., Fischbach-Teschl, C., Lpez, J.A., Stroock, A.D., 2012. *In vitro microvessels for the study of angiogenesis and thrombosis.* Proc. Natl. Acad. Sci. U.S.A., 109, 9342–9347.

RECENT REPORTS

12/55	Thermoviscous Coating and Rimming Flow	Leslie Wilson Duffy
12/56	On the anomalous dynamics of capillary rise in porous media	Shikhmurzaev Sprittles
12/57	Compactly supported radial basis functions: how and why?	Zhu
12/58	Multiscale reaction-diffusion algorithms: pde-assisted Brownian dynamics	Franz Flegg Chapman Erban
12/59	Numerical simulation of shear and the Poynting effects by the finite element method: An application of the generalised empirical inequalities in non-linear elasticity	Mihai Goriely
12/60	From Brownian dynamics to Markov chain: an ion channel example	Chen Erban Chapman
12/61	Three-dimensional coating and rimming flow: a ring of fluid on a rotating horizontal cylinder	Leslie Wilson Duffy
12/62	A two-pressure model for slightly compressible single phase flow in bi-structured porous media	Soulaine Davit Quintard
12/63	Mathematical modelling plant signalling networks	Muraro Byrne King Bennett
12/64	A model for one-dimensional morphoelasticity and its application to fibroblast-populated collagen lattices	Menon Hall McCue McElwain
12/65	Effective order strong stability preserving RungeKutta methods	Hadjimichael Macdonald Ketcheson Verner
12/66	Morphoelastic Rods Part I: A Single Growing Elastic Rod	Moulton Lessinnes Goriely
12/67	Wrinkling in the deflation of elastic bubbles	Aumaitre Knoche Cicuta Vella
12/68	Indentation of ellipsoidal and cylindrical elastic shells	Vella Ajdari Vaziri Boudaoud

12/71	The Mathematics Behind Sherlock Holmes: A Game of Shadows	Goriely Moulton
12/72	Some observations on weighted GMRES	Güttel Pestana
12/73	Bounds on the solution of a Cauchy-type problem involving a weighted sequential fractional derivative	Furati
12/74	Static and dynamic stability results for a class of three-dimensional configurations of Kirchhoff elastic rods	Majumdar Goriely
12/75	Error estimation and adaptivity for incompressible, nonlinear (hyper)elasticity	Whiteley Tavener
12/76	A note on heat and mass transfer from a sphere in Stokes flow at low Péclet number	Bell Byrne Whiteley Waters
12/77	Effect of disjoining pressure in a thin film equation with non-uniform forcing	Moulton Lega

Copies of these, and any other OCCAM reports can be obtained from:

Oxford Centre for Collaborative Applied Mathematics
Mathematical Institute
24 - 29 St Giles'
Oxford
OX1 3LB
England
www.maths.ox.ac.uk/occam